Advanced Integrative Multiscale Modeling System for Countering the Threat of CBRN Terrorism

Eugene Yee
Defence R&D Canada – Suffield
P.O. Box 4000, STN MAIN
Medicine Hat, Alberta, T1A 8K6
CANADA

Richard Hogue
Canadian Meteorological Centre
2121 TransCanada Highway
North Service Road
Dorval, Quebec, H9P 1J3
CANADA

email: eugene.yee@drdc-rddc.gc.ca

email: richard.hogue@ec.gc.ca

Abstract

A comprehensive overview of the prognostic physics-based models for urban flow and dispersion that have been developed as part of a four-year research and development effort is described. The effort was funded by the **C***hemical, Biological, Radiological and Nuclear (CBRN)* **R***esearch and* **T***echnology* **I***nitiative (CRTI) under a project entitled "An Advanced Emergency Response System for CBRN Hazard Prediction and Assessment for the Urban Environment". The primary objective of this project was to develop an advanced, high-fidelity, fully validated, state-of-the-science modeling system for the prediction of urban flows and the dispersion of CBRN agents released in these highly disturbed flows. This paper provides a general overview of the development of this comprehensive integrative multiscale CBRN modeling and simulation capability. This capability allows CBRN materials to be tracked from the near field (street or building scale to the microscale), through the intermediate field (mesoscale), to the far field (regional or continental scale) and finally out to the very far field (synoptic and global scales) at the appropriate resolution for each length (and associated time) scale. This unique modeling/simulation system consists of 4 major components: (1) development of models for the prediction of building-aware flows in urban areas at the microscale; (2) inclusion of subgrid scale urban parameterizations in a mesoscale numerical weather prediction*

model (Global Environmental Multiscale or GEM, and its limited area version GEM LAM); (3) coupling of the urban microscale model for building-aware flow prediction with the "urbanized" mesoscale model; and, (4) development of Eulerian and Lagrangian stochastic (LS) models for the prediction of urban dispersion which are "driven" by the multiscale wind flow and turbulence models described above. The integrative multiscale CBRN modeling and simulation system has been validated by comparing model predictions with comprehensive experimental data sets obtained from laboratory studies of flow and dispersion over idealized obstacle arrays and from a full-scale urban field experiment conducted in Oklahoma City, Oklahoma in July 2003 (Joint Urban 2003, or JU2003).

1.0 INTRODUCTION

The environmental and toxiological impact of the downwind transport and diffusion of contaminants released into the atmosphere has become increasingly important in recent years. Considerable interest has been focused on the prediction of mean concentration levels downwind of contaminant sources in the turbulent atmospheric boundary layer. Consequently, atmospheric transport and diffusion models have played an important role in emergency response systems for toxic releases and have been used in calculating the transport, diffusion, and deposition of toxic chemical, biological, or radiological materials released (either accidentally or deliberately) into the turbulent atmospheric boundary layer over relatively smooth and horizontally homogeneous surfaces. For example, military and civilian (government and commercial) emergency response models commonly use standard Gaussian plume or puff models, which employ semi-empirical relationships for plume or puff growth with the mean wind and turbulence field obtained either from similarity theory or from the use of simple diagnostic wind fields constructed from interpolation and/or extrapolation of sparse observational data. The advantages of these approaches for wind flow specification are their simplicity, general applicability in simple atmospheric conditions, and most importantly, their limited computational requirements. While this approach is useful for a landscape that is relatively flat and unobstructed, it is wholly inadequate for surface-atmosphere interactions over "complex" surfaces (viz., most of the real world) such as cities and other built-up areas.

It needs to be emphasized that as the fraction of the World's population that live in cities continues to grow, it is becoming increasingly important to address the urgent problem of modeling of the dispersion of toxic releases in the urban environment, characterized by extremely diverse length and time scales and complex geometries and interfaces. Indeed, a typical urban canopy consists of a large collection of buildings and other obstacles (e.g., cars lining a street, treed areas in city green spaces, etc.) that are aggregated into complex structures. When this rough surface interacts with the atmospheric flow within and above it, the disturbed flow field can become extremely complex (e.g., curved mean streamlines, large velocity gradients, sharp velocity discontinuities, flow separations and reattachments, cavity regions, recirculation zones, and strongly inhomogeneous turbulence). Understanding the complex flow of the wind through and above the urban environment and the dispersion of contaminants released into that flow is both necessary and important. In view of

this, we require physically-based urban wind models that can provide the needed spatial-temporal pattern of urban wind statistics required to "drive" modeling of dispersion of contaminants within the street canyons of an urban environment (where it is venting of these street canyons that is important for determination of the contaminant concentrations).

The United States Government Accountability Office (GAO) recently conducted a review of various models used by federal agencies to predict the transport and dispersion of terrorist-related and accidental releases of chemical, biological, radiological and nuclear (CBRN) materials in urban areas [1]. Based on that review, it was concluded that "evaluations and field testing of plume models developed for urban areas show variable predictions in urban environments" and that "federal agencies' models to track the atmospheric release of CBRN materials have major limitations in urban areas". In addition to these deficiencies, the GAO report [1] also cautioned the reader that using predictions of non-urban plume models for CBRN events in urban areas "are limited in their ability to accurately predict the path of a plume and the extent of contamination in urban environments".

This identified capability gap (which has been generally acknowledged by various dispersion modeling experts) was the motivation for the development of an advanced emergency response system for CBRN hazard prediction and assessment for the urban environment sponsored by **C**hemical, Biological, Radiological and Nuclear **R**esearch and **T**echnology **I**nitiative (CRTI) under Project 02-0093RD entitled "An Advanced Emergency Response System for CBRN Hazard Prediction and Assessment for the Urban Environment". The principal objective of this project was to develop an advanced, fully validated, state-of-the-science modeling system for the prediction of urban flow (i.e., turbulent flow through cities) and the concomitant problem of the modeling of the dispersion of CBRN agents released into these complex flows. This system allows the dispersion of CBRN materials to be modeled over a vast range of length scales at the appropriate resolution for each scale: namely, in the near field (up to about 2 km) where dispersion is governed by the micro-scale regime of the planetary boundary layer; to the intermediate field between about 2 and 20 km where dispersion is governed by the local or meso-γ scale; through the far field covering the range from about 20-200 km (meso-β scale) and from about 200–2000 km (meso-α scale) which correspond to dispersion at the regional scale; and, finally out to the very far field encompassing scales greater than about 2000 km corresponding to dispersion on the large (synoptic and global) scales.

The development of this proposed high-fidelity, multiscale and multi-physics modeling system will provide a real-time modeling and simulation tool for prediction of injuries, casualities, and contamination resulting from the release of a CBRN agent in an urban area. This, in turn, will provide the key-enabling technology that will enable emergency managers and decision makers to make the informed decisions (based on the strongest technical and scientific foundations) required in the support of Canada's more broadly based efforts at advancing CBRN counter-terrorism planning and operational capabilities.

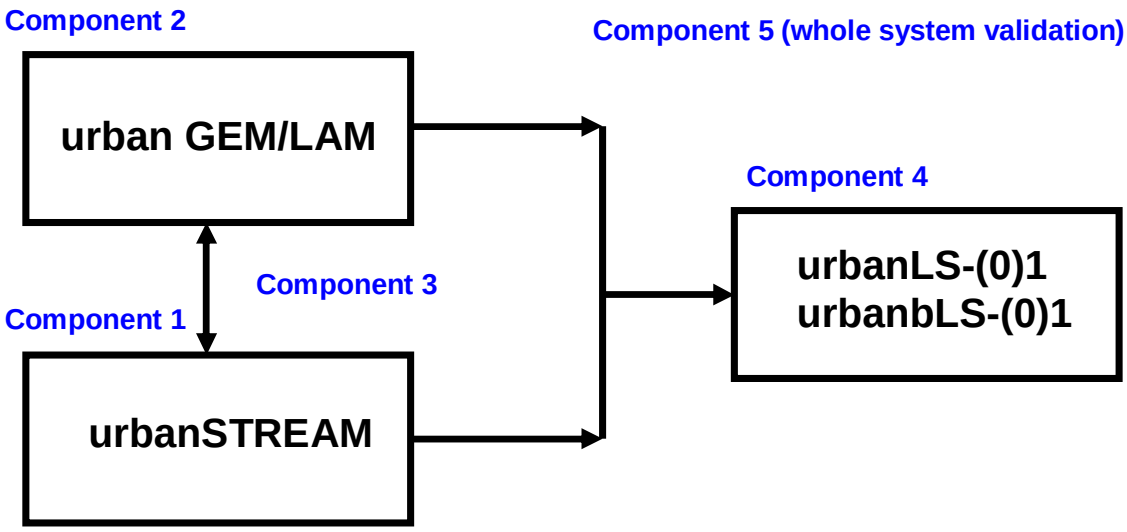

Figure 1: Relationships between various components of CRTI Project 02-0093RD.

The multiscale modeling system for emergency response consists of five major components shown in the schematic diagram of Figure 1. These five components can be described briefly as follows. Component 1 involves the development of models to predict the mean flow and turbulence in the urban complex at the microscale (from the building and street scale up to a length scale of about 2 km). Two kinds of models have been developed for this purpose: namely, high-resolution building-aware models for urban flow where buildings are explicitly resolved; and, virtual building models for urban flow where groups of buildings are represented simply in terms of a distributed drag force. This component involves also the development of Eulerian models for urban dispersion, which interface directly with the microscale urban flow model.

Component 2 involves the inclusion of the effects of urban terrain on the subgrid scales of a mesoscale meteorological model through an urban parameterization. This parameterization is required to account properly for the area-averaged effects of form drag, increased turbulence production, heating and surface energy budget modification due to the presence of buildings/obstacles and urban land use within the urban environment. Component 3 involves coupling the urban microscale flow models developed in Component 1 with the "urbanized" mesoscale model developed in Component 2. The interface between the urban microscale flow models and the "urbanized" GEM LAM model is demanding in that the information transfer between the two models must honor physical conservation laws, mutually satisfy mathematical boundary conditions, and preserve numerical accuracy, even though the corresponding meshes might differ in structure, resolution, and discretization methodology.

Component 4 involves using the mean flow and turbulence predicted by the multiscale flow model developed in Component 3 to "drive" Lagrangian stochastic (LS) model for the prediction of urban dispersion of CBRN agents. The application of LS models to atmospheric dispersion in general (and, urban dispersion in particular) is recommended over Eulerian models because LS models (1) are (in principle) the most flexible and the most easily able to incorporate all the known statistical details of the complex urban flow and (2) are physically transparent, and easily adapted to handle particulates, biological or radioactive decay, dry and wet deposition, and other relevant source and sink mechanisms. However, an Eulerian model of dispersion for the urban environment is easier to implement and requires less computational effort than an LS model, so both types of dispersion models are made available within the integrative multiscale modeling system. Finally, Component 5 involves a validation of the multiscale modeling system for both the urban flow and dispersion components.

2.0 LARGE-SCALE ENVIRONMENTAL FLOW MODEL

The prediction of large-scale environmental flows is based on a comprehensive and fully-integrated global atmospheric forecasting and simulation system developed by Meteorological Research Branch and Canadian Meteorological Centre [2,3]. This model is known by the acronym GEM LAM which refers to "the **G**lobal **E**nvironmental **M**ultiscale model which encompasses **L**ocal **A**rea **M**odeling". As the name implies, GEM LAM is designed to model atmospheric phenomena covering a wide range of temporal and spatial scales, from the meso-γ regime involving scales of several hundred metres right through to the global scale of tens of thousamds of kilometres, within one consistent and universal modeling framework. In consequence, this modeling framework is capable of meeting the weather forecasting needs, both operational and research, of Canada while simultaneously providing the capability to cope with air quality and climate modeling needs.

The GEM LAM modeling schemata allows variable resolution over the globe to be achieved using the formulation proposed by Côté et al [4] which permits the resolution to be simultaneously varied in the north-south and east-west coordinate directions in a flexible manner. The formulation utilizes a regular (but variable resolution) latitude-longitude gird that can be arbitrarily rotated. The ability to rotate the grid allows the resolution to the be focused over any user-selected area of the Earth. Moreover, the regularity of the latitude-longitude grid facilitates computational efficiency, owing to the fact that this regularity is reflected in the simple structure of the resulting discretized matrix equations for which efficient solvers are available.

The flexibility of the spherical geometry variable-resolution grid used in GEM LAM allows different grid configurations to be designed for different applications. Figure 2 exhibits several uniform- or variable-resolution horizontal grid configurations, demonstrating the flexibility of this gridding approach. The first of these, shown on the left-hand side, corresponds to a uniform-resolution mesh over the entire globe to give a resolution of 33 km. This grid can be used to model atmospheric

phenomena on a synoptic and global scale. The second grid configuration, shown in the middle panel of Figure 2, consists of a 289×289 variable-resolution horizontal mesh that is used currently in the operational configuration of the GEM LAM model. This grid has a uniform resolution of 15 km over a $50^\circ \times 77.22^\circ$ (180×235) region of the globe centred on North America. This grid configuration is suitable for regional-scale problems. Finally, the third grid configuration shown on the right-hand side of Figure 2, illustrates a meso-γ mesh with a resolution that can be varied between 2.5 and 1 km depending on the specific application. In the example, the highly-focused uniform mesh is centred over the Vancouver-Whistler area. The resolution is seen to vary smoothly away from the uniform-resolution subdomain, with an approximately 10% successive increase in mesh length as used in the regional configuration (middle panel). This grid configuration is suitable for the simulation of terrain-induced mesoscale systems (e.g., forced airflow over and around rough terrain, offshore-onshore flow patterns over the land-sea interface) or of urban circulations due to the differential heating and cooling between the rural and urban areas that generate and sustain these wind systems.

The governing equations underpinning the GEM LAM model are the fully compressible forced non-hydrostatic Euler equations. This system includes transport equations for the horizontal and vertical momentum, continuity, energy and moisture equations, and the equation of state. These are the appropriate equations for smaller-scale applications where the neglect of the vertical acceleration in the prognostic vertical momentum equation cannot be justified. For larger- and synoptic-scale applications, the vertical accleration can be neglected with the consequence that the hydrostatic approximation can be used to an excellent approximation. In this flow regime, the governing equations reduce to the hydrostatic primitive equations in which pressure is determined using the diagnostic hydrostatic equation.

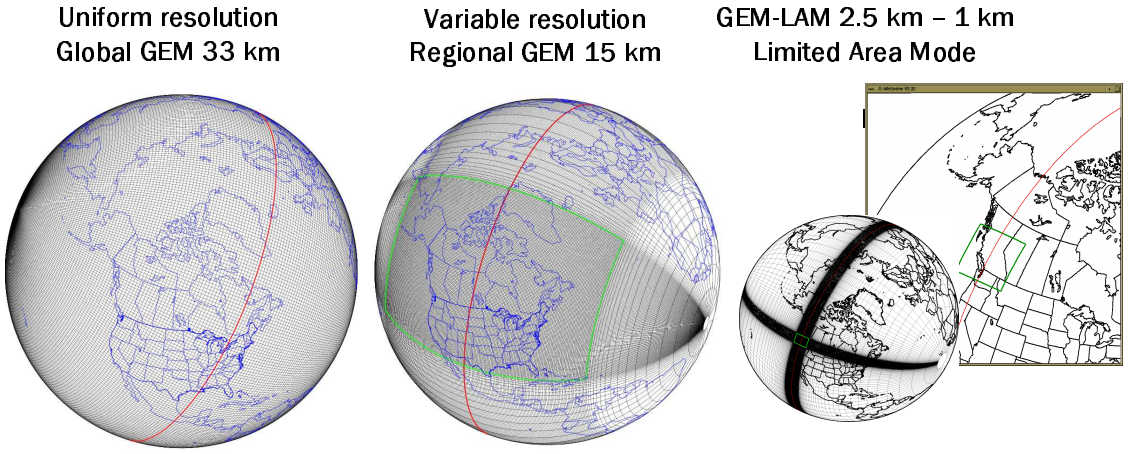

Figure 2: Illustration of the global variable resolution grids that are available within the integrated atmospheric environmental forecasting and simulation system known as GEM LAM.

The grid-volume averaging of the governing equations used in GEM LAM results in averaged subgrid-scale correlation terms and averaged source-sink (forcing) terms. Parameterizations are required to specify these subgrid scale and source-sink terms in order to "close" the conservation equations. To accomplish this, the GEM LAM model has been interfaced with the Recherche en Prévision Numérique (RPN) physics package, using the RPN standardized interface. This interface allows the immediate (re)-use of a tested set of parameterizations without any re-tuning, although the choice of the parameterization depends on the temporal and spatial scales of the application and the resolution of the simulation or forecast. Parameterizations in the RPN package [5] are available for a number of physical phenomena:

- condensation;
- precipitation including evaporative effects;
- solar and infrared readiation with or without cloud interaction;
- deep and shallow convection;
- prognostic clouds;
- gravity wave drag;
- surface-layer effects, including land surface parameterization; and,
- turbulent fluxes of momentum, heat and moisture over land, water and ice, based on prognostic turbulent kinetic energy.

The governing equations of the GEM LAM model are first integrated without the forcing terms, and the parameterized forcing terms are then computed and added using the standard fractional-step time integration method. An implicit treatment of the non-advective terms in the conservation equations, governing the fasting-moving acoustic and gravitational oscillations, is used. A semi-Lagrangian treatment is used for the advection processes in order to overcome the stability limitations on the size of the time step encountered in usual Eulerian schemes. A grid-volume averaged finite-element discretization is applied to provide a robust methodology for achieving variable mesh resolution.

2.1 Urbanized GEM LAM

The representation of urban surfaces (over cityscapes) as a bottom boundary condition in GEM LAM requires different types of models than those required to represent rural land covers. Urban surfaces are generally composed of buildings and discrete street canyons. Owing to the complexity of the urban morphology, the near-surface (lower) atmospheric flow and the thermal structure are significantly influenced by the underlying obstacles. Furthermore, the resolution available to GEM

LAM precludes (at this time) the explicit inclusion of buildings into the weather model. As a consequence, the "urbanized" version of GEM LAM includes instead, a land surface parameterization scheme for urban surfaces. This urban parameterization scheme simulates the turbulent fluxes into the atmosphere at the surface of the GEM LAM model covered by buildings, roads, or any artifical (man-made) material. The scheme parameterizes both the urban surface and the roughness sublayer above it.

The urbanized GEM LAM model includes the complex processes of urban surface conditions through the use of a single-layer urban-canopy formulation proposed by Masson [6] and Masson et al. [7]. This urban parameterization scheme, known as the Town Energy Balance (TEB) scheme, is illustrated in Figure 3. A grid cell in GEM LAM is fractionally divided into different types of land and water cover (e.g., vegetation, bare soil, water, built-up or urban canyon area). The urban canyon fraction is composed of the paved road, two facing building walls, and the rooftops of these buildings. The rooftop is assumed to be at the surface level of the atmospheric (GEM LAM) model. It is assumed implicitly that the effects of road (or canyon) orientation have been averaged over all possible orientations, which exist with the same (uniform) probability (viz., isotropy of the street orientations is assumed).

Possible energy exchange pathways are represented in Figure 3: roof-reference atmosphere, canopy air-reference atmosphere, wall-canopy air, and road-canopy air. Artificial surface temperatures and interior heat fluxes are calculated by solving one-dimensional thermal conductance equations that have a multi-layer, variable vertical grid spacing. Anthropogenic sources of heat and humidity (e.g., domestic heating, combustion sources from traffic and industry) are considered in the TEB scheme. Finally, the urban parameterization accounts for water budgets on the various artificial surfaces, which is known to play an important role in the surface energy budget. More specifically, when the surface is wet, the latent heat flux will be increased, which enhances the humidity and reduces the temperature of the ambient air relative to the dry surface condition.

2.2 Urban Cover Classification

Detailed data describing the complex urban surface geometry are needed to initialize the input parameters required by the TEB scheme. These parameters can be obtained from land-use and land-cover (LULC) databases that contain the required information on the spatial variability of the surface properties (and, more particularly, the urban surface properties within a given cityscape). Unfortunately, at this moment, no comprehensive databases for land-use and land-cover are available for Canadian cities. Because of the lack of LULC databases for Canadian cities, Meteorological Service of Canada initiated a research and development effort to develop a general methodology for producing semi-automated urban LULC classifications in major Canadian cities (or, any city in any country, for that matter).

To specify the urban parameters needed by the urban canopy-layer scheme TEB, two semi-

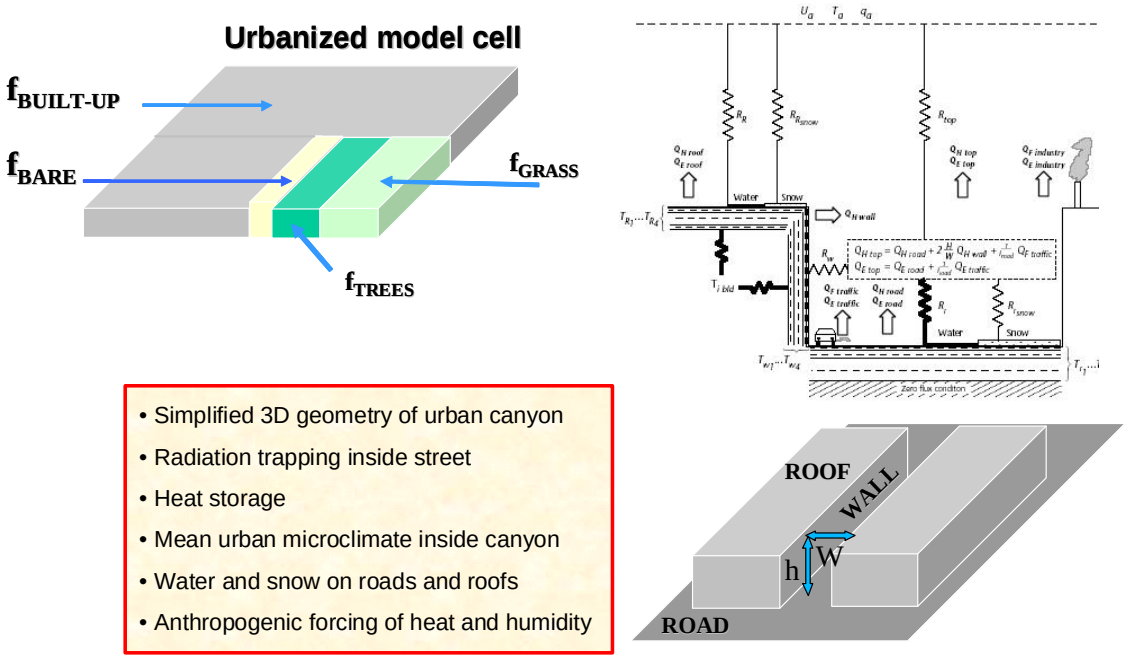

Figure 3: Schematic diagram of the urban canopy parameterization (Town Energy Balance, or TEB scheme) indicating the pathways of momentum, heat and moisture from/to various surfaces (roof, wall, and road). The TEB scheme accounts explicitly for radiation trapping and shadow effects, heat storage in the urban fabric, mean wind, temperature and humidity inside the urban canyon, and water and snow on roofs and streets.

automatic methods [8] have been developed to derive land-use and land-cover urban classifications for the major Canadian (or North American) cities. The first method is based on the joint analysis of satellite imagery and digital elevation models. The second method uses vector data from the National Topographic Database. For the first method, the application of a decision tree model allows the identification of 12 urban classes, that are representative of the urban cover variability for North American cities. These methods have been applied successfully to produce a database of urban LULC for Oklahoma City, Montreal and Vancouver. The methodology is general and can be easily applied to other cities in Canada or in other countries. An example of the urban cover classification obtained for Vancouver using the semi-automatic processing methodology is exhibited in Figure 4.

3.0 BUILDING-AWARE URBAN FLOW MODEL

The integrative multiscale urban model system includes a component for the provision of a building-aware urban flow model. This component includes five main modules: urbanGRID, ur-

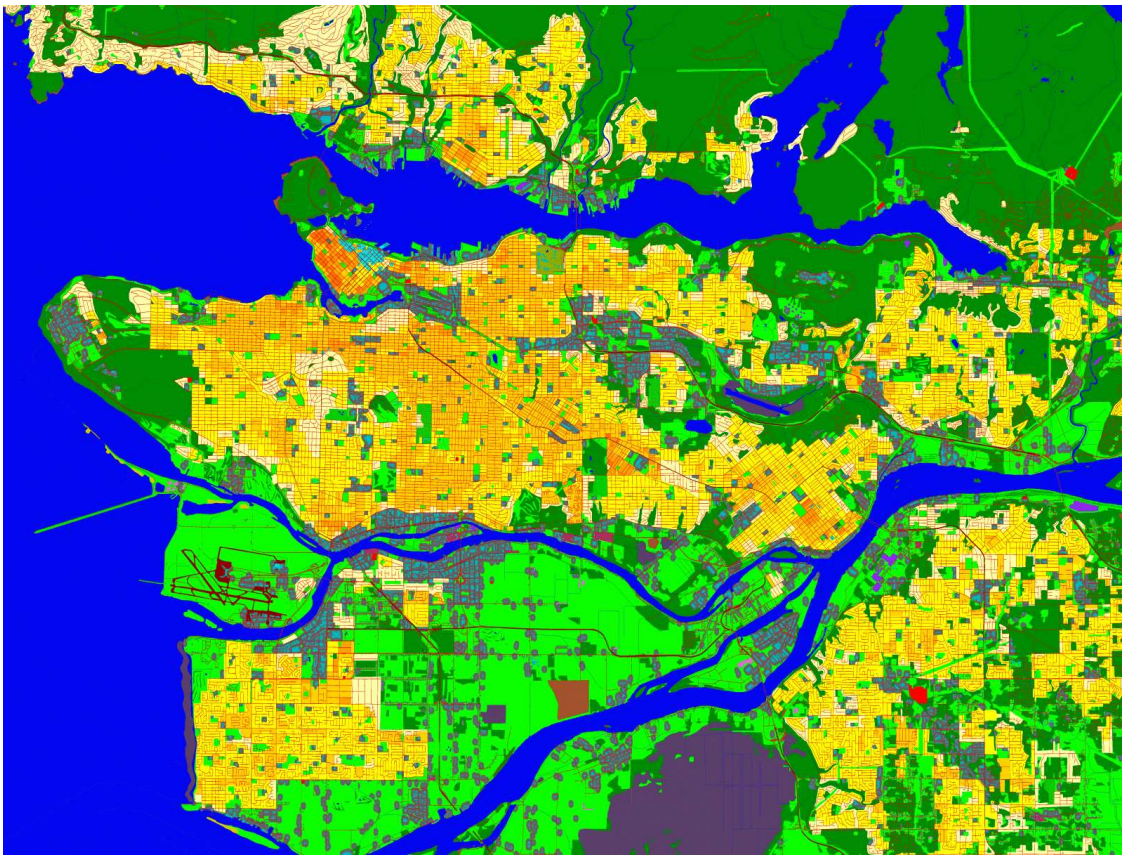

Figure 4: Land-cover and land-use classification over the city of Vancouver, British Columbia.

banSTREAM, urbanEU, urbanAEU, and urbanPOST. These modules and how they interface with each other and with other project components are shown in Figure 5. For a detailed technical description of the modules that comprise Component 1 of the multiscale urban modeling system, the reader is referred to Yee et al. [9].

In the simplest terms, urbanGRID imports building information encoded in Environmental Systems Research Institute (ESRI) Shapefiles and uses this data to generate a structured grid over a user-selected computational domain in a given cityscape. Furthermore, urbanGRID imports three-dimensional meteorological fields (e.g., mean wind, turbulence kinetic energy, etc.) provided by urban GEM LAM and uses this information to provide inflow boundary conditions for the urban microscale (or, building-aware) flow model.

The structured grid and inflow boundary conditions provided by urbanGRID are used as input by

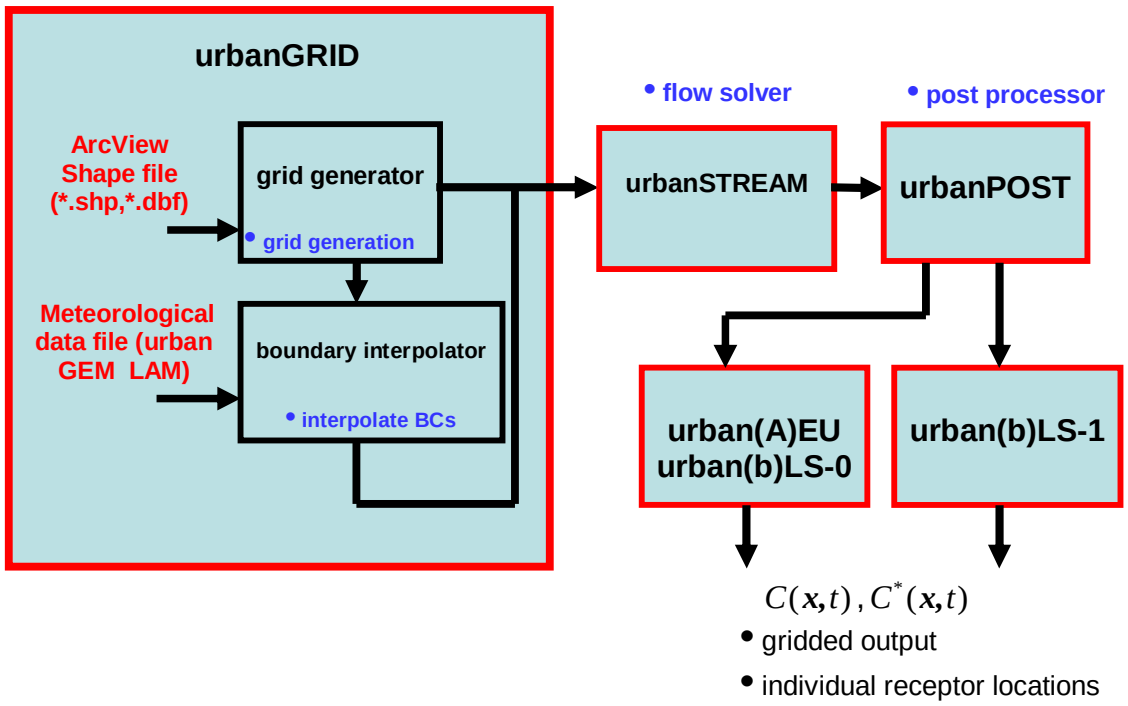

Figure 5: Various modules of Component 1 and their relationship to other components of CRTI Project 02-0093RD.

urbanSTREAM which is a computational fluid dynamics (CFD) model for the numerical simulation of the flows within and above the complex geometries of buildings in the cityscape. The flow solver urbanSTREAM provides the high-resolution wind and turbulence fields used by the two Eulerian grid dispersion models urbanEU (source-oriented) and urbanAEU (receptor-oriented) to simulate the dispersion of contaminants in the urban area. These two urban dispersion models are based on the numerical solution of a K-theory advection-diffusion equation or its adjoint. Finally, urbanPOST is used to post-process the primary output files from urbanSTREAM to provide an appropriate specification of wind statistics required as input by either the two Eulerian urban dispersion models urbanEU and urbanAEU or, alternatively, by the urban Lagrangian stochastic particle trajectory model urbanLS (forward dispersion model) or urbanbLS (backward dispersion model) developed under Component 4 of CRTI Project 02-0093RD. Both zeroth-order forward and backward Lagrangian stochastic models (or, random displacement models) involving the evolution of the position of a "marked" fluid particle (urban(b)LS-0) and first-order forward and backward Lagrangian stochastic models involving the joint evolution of the position and velocity of a "marked" fluid particle (urban(b)LS-1) have been formulated.

3.1 Automatic grid generation in urban areas: urbanGRID

urbanGRID is a program that is concerned with the automatic generation of structured grids (or meshes) in the computational domain for numerical solutions involving the complex geometry of buildings and other obstacles in the urban environment (real cityscape). This program provides a predetermined mesh which fills the entire computational domain, and serves as the input data for spatial discretization required to "drive" the flow solver program urbanSTREAM. The mesh determines the location in the domain at which the flow quantities will be evaluated, as well as where boundary conditions need to be applied at all the walls and roofs of arbitrary-shaped buildings (and other solid surfaces) in the domain.

The geometric information on shapes and locations of buildings in the computational domain (corresponding to a region of a real city) is assumed to be available in form of ESRI Shapefiles [10]. An ESRI Shapefile is a digital vector storage format that stores non-topological information and spatial features in a data set, with the geometry for each feature comprising a set of vector coordinates and associated attribute information.

The computational domain where the flow field will be calculated is specified by the user who provides the x and y coordinates (easting and northing coordinates, respectively) of the southwest ($x_{\mathrm{SW}}^{\mathrm{outer}}$, $y_{\mathrm{SW}}^{\mathrm{outer}}$) and northeast ($x_{\mathrm{NE}}^{\mathrm{outer}}$, $y_{\mathrm{NE}}^{\mathrm{outer}}$) corners of the domain in the Universal Transverse Mercator (UTM) coordinate system. Additionally, the user provides the easting and northing coordinates of the southwest ($x_{\mathrm{SW}}^{\mathrm{inner}}$, $y_{\mathrm{SW}}^{\mathrm{inner}}$) and northeast ($x_{\mathrm{NE}}^{\mathrm{inner}}$, $y_{\mathrm{NE}}^{\mathrm{inner}}$) corners for an inner domain which lies strictly inside the computational domain, where buildings are explicitly resolved (building-aware region) in the sense that appropriate boundary conditions are imposed on all the building surfaces (e.g., wall, roofs). For the region that lies outside the inner domain but inside the computational domain, the buildings are treated as virtual in the sense that the effects of these unresolved buildings on the flow are represented simply as a distributed mean-momentum sink in the mean momentum equation (which is described later in this paper). urbanGRID uses the Shapefile C Library Version 1.2 [11] for reading ESRI Shapefiles, and of greatest interest here, are the vector coordinates of all the vertices (ordered in a counter-clockwise direction) that define the footprints of the buildings (which are represented in UTM coordinates) and the attribute corresponding to the heights of the buildings in the inner domain. Finally, the height z_d of the computational domain is provided as a user input to urbanGRID.

Once the computational domain has been defined, a structured Cartesian mesh is generated over the domain. The implicit grid structure alleviates the need to store the mesh connectivity, and permits the use of rapid iterative solution algorithms for the computation of the flow, which makes use of sparse matrix solvers. urbanGRID generates a Cartesian mesh over the computational domain by defining an arrangement of discrete grid points that define the cell faces (grid lines). In any given coordinate direction, the spacing of the grid points starting from a solid surface (e.g., ground surface, wall or roof of a building, etc.) is stretched as one moves away from the surface along the

coordinate direction.

In the inner region of the computational domain, the buildings are explicitly resolved and it becomes imperative to define an appropriate data structure to encode information about whether a control volume (grid cell) is a fluid cell (which lies mostly or completely within the fluid region) or an obstacle cell (which lies mostly or completely inside a building), and if a fluid cell whether any face of this cell abuts against a wall or roof of a building (the latter information being required for the implementation of the wall function boundary condition in urbanSTREAM). To this purpose, urbanGRID uses an 8-bit integer `FLAG` array to encode this information.

Because each building extracted from an ESRI Shapefile has a constant height attribute, it is computationally more efficient to consider the intersection of the projection of the cell in the horizontal x-y plane with the building footprint (represented by a closed-loop polygon in the Shapefile) in order to determine whether a particular grid cell is a fluid cell or an obstacle cell. To this end, a bounding box (or, smallest rectangle that completely surrounds the building footprint and has sides that are parallel to the x-axis and y-axis) is constructed for each building within the inner (or, building-aware) region. Clearly, only grid cells that intersect any of these bounding boxes in the inner region can possibly be classified as obstacle cells (with the appropriate bit in the associated `FLAG` array set); otherwise, the grid cell must necessarily be classified as a fluid cell.

The distribution of flow variables needs to be specified (viz., Dirichlet boundary conditions need to be defined) at the inflow boundary planes for the computational domain used for flow calculation in urbanSTREAM. To this purpose, urbanGRID interpolates the gridded mean velocity and turbulence fields provided by urban GEM LAM (a prognostic mesoscale model with an urban parameterization developed by Environment Canada for CRTI Project 02-0093RD). The gridded mean velocity and turbulence kinetic energy fields provided by urban GEM LAM in a large domain that includes the computational domain defined in urbanGRID are linearly interpolated to the grid nodes in the inflow boundary planes for urbanSTREAM. This corresponds to a one-way coupling (down-scaling) between the mesoscale flow model urban GEM LAM and the microscale (building-aware) flow model urbanSTREAM.

3.2 Flow solver: urbanSTREAM

The computational fluid dynamics (CFD) code urbanSTREAM was developed specifically in a general non-orthogonal (curvilinear) coordinate system in order to compute specifically the flow through and above an urban canopy on arbitrary terrain. The curvilinear coordinate system allows the terrain to be described accurately. However, for simplicity of exposition, the relevant governing flow equations will be stated in a Cartesian orthogonal coordinate system, despite the fact that the flow solver has been implemented in a general curvilinear coordinate system.

The prediction of the complex flow (mean wind and turbulence quantities), through and above an

urban canopy consisting of groups of buildings in various configurations that are representative of a real cityscape, is based on the Reynolds-averaged Navier-Stokes (RANS) equations whereby the turbulent flow is considered as consisting of two components: a fluctuating part and a mean or average part. The Reynolds-averaged continuity and momentum equations for an incompressible adiabatic (i.e., not buoyancy-affected) fluid are a system of partial differential equations governing mass and momentum conservation and can be expressed in Cartesian coordinates as follows:

Continuity

$$\frac{\partial \bar{u}_i}{\partial x_i} = 0, \tag{1}$$

Momentum

$$\frac{\partial \bar{u}_i}{\partial t} + \frac{\partial \bar{u}_j \bar{u}_i}{\partial x_j} = -\frac{\partial \bar{p}}{\partial x_i} + \nu \frac{\partial^2 \bar{u}_i}{\partial x_j^2} - \frac{\partial}{\partial x_j}(\overline{u_i' u_j'}) - 2\epsilon_{ijk}\Omega_j \bar{u}_k, \tag{2}$$

where the Reynolds averaging of a quantity is denoted by drawing a bar over the quantity. Summation is implied by repeated indices. Here, $\bar{u}_i$ and u_i' are the mean and fluctuating velocities in the x_i-direction, respectively, with $i = 1$, 2, or 3 representing the west-east x, south-north y, or vertical z directions; $x_i = (x, y, z) \equiv \mathbf{x}$; t is time; $u_i = (u, v, w)$; $\bar{u}_i = (\bar{u}, \bar{v}, \bar{w})$;[1] ν is the kinematic viscosity and $\bar{p}$ is the kinematic mean pressure (with p' used to denote pressure fluctuations). The last term on the right-hand-side of Equation (2) is the Coriolis acceleration term (caused by the Coriolis force) where Ω_j is the Earth's rotation vector and ϵ_{ijk} is the permutation symbol [which has the value zero if any pair of subscripts is identical, and is $(-1)^q$ otherwise where q is the number of subscript transpositions required to bring (ijk) to the natural order (123)].

The Boussinesq eddy-viscosity approximation is used to model the kinematic Reynolds stresses and, hence, close the system of equations. This approximation, which is perhaps the simplest coordinate invariant relationship between stresses and strains, assumes the following form:

$$\overline{u_i' u_j'} = \frac{2}{3} k \delta_{ij} - \nu_t \left(\frac{\partial \bar{u}_i}{\partial x_j} + \frac{\partial \bar{u}_j}{\partial x_i} \right), \tag{3}$$

where ν_t is the kinematic eddy viscosity, $k \equiv \frac{1}{2}\overline{u_i' u_i'}$ is the turbulence kinetic energy (TKE), and δ_{ij} is the Kronecker delta function. The CFD code urbanSTREAM also implements a more sophisticated turbulence closure scheme for the kinematic Reynolds stresses $\overline{u_i' u_j'}$. To this purpose, there is an option in the code to approximate $\overline{u_i' u_j'}$ using an explicit nonlinear algebraic Reynolds stress model proposed originally by Speziale [12]: namely,

$$\begin{aligned} \overline{u_i' u_j'} \;=\; & \frac{2}{3} k \delta_{ij} - \nu_t \left(\frac{\partial \bar{u}_i}{\partial x_j} + \frac{\partial \bar{u}_j}{\partial x_i} \right) + \frac{k^3}{\epsilon^2} \left[C_{\tau 1} \left(\frac{\partial \bar{u}_i}{\partial x_k} \frac{\partial \bar{u}_j}{\partial x_k} \right)^* \right. \\ & \left. + C_{\tau 2} \left(\frac{\partial \bar{u}_i}{\partial x_k} \frac{\partial \bar{u}_k}{\partial x_j} + \frac{\partial \bar{u}_j}{\partial x_k} \frac{\partial \bar{u}_k}{\partial x_i} \right)^* + C_{\tau 3} \left(\frac{\partial \bar{u}_k}{\partial x_i} \frac{\partial \bar{u}_k}{\partial x_j} \right)^* \right], \end{aligned} \tag{4}$$

[1] with the implied Reynolds decomposition $u_i = \bar{u}_i + u_i'$.

where an asterisk is used to indicate the deviatoric part of a tensor (viz., $(\cdot)^*_{ij} \equiv (\cdot)_{ij} - (\cdot)_{kk}\delta_{ij}/3$), and ϵ denotes the viscous dissipation rate for TKE. The three model coefficients appearing in this equation have the following values: $C_{\tau 1} = 0.041$, $C_{\tau 2} = 0.014$ and $C_{\tau 3} = -0.014$. Note that the first two terms in the nonlinear Reynolds stress model of Equation (4) are simply the Boussinesq approximation for $\overline{u_i' u_j'}$.

For both the linear (or, Boussinesq) and nonlinear models for the Reynolds stresses, the task of turbulence closure reduces to the determination of the eddy viscosity ν_t. In the most common approach, the turbulence velocity and length scales that determine ν_t are based on the turbulence kinetic energy k and its dissipation rate ϵ (i.e., rate at which TKE is converted into thermal internal energy), with

$$\nu_t = C_\mu \frac{k^2}{\epsilon}, \tag{5}$$

where C_μ is a closure constant. This is the so-called k-ϵ modeling framework at high-Reynolds (high-Re) numbers. To complete the formulation of ν_t, we need transport equations for k and ϵ.

The modeled transport equation for the turbulence kinetic energy k is

$$\frac{\partial k}{\partial t} + \frac{\partial \bar{u}_j k}{\partial x_j} = \frac{\partial}{\partial x_j}\left[\left(\nu + \frac{\nu_t}{\sigma_k}\right)\frac{\partial k}{\partial x_j}\right] + P_k - \epsilon, \tag{6}$$

where P_k is the production of k defined as

$$P_k \equiv -\overline{u_i' u_j'}\frac{\partial \bar{u}_i}{\partial x_j}. \tag{7}$$

The modeled equation for the TKE dissipation rate ϵ has the following form:

$$\frac{\partial \epsilon}{\partial t} + \frac{\partial \bar{u}_j \epsilon}{\partial x_j} = \frac{\partial}{\partial x_j}\left[\left(\nu + \frac{\nu_t}{\sigma_\epsilon}\right)\frac{\partial \epsilon}{\partial x_j}\right] + \frac{\epsilon}{k}(C_{\epsilon 1} P_k - C_{\epsilon 2}\epsilon), \tag{8}$$

where $C_{\epsilon 1}$, $C_{\epsilon 2}$, σ_k and σ_ϵ are closure constants to be determined.

Together, the transport equations for k and ϵ contain five closure constants (C_μ, σ_k, σ_ϵ, $C_{\epsilon 1}$, and $C_{\epsilon 2}$) which must be determined before the equations can be solved. Following the recommendations of Launder and Spalding [13], the closure coefficients for the standard k-ϵ turbulence model are

$$C_\mu = 0.09, \quad \sigma_k = 1, \quad \sigma_\epsilon = 1.3, \quad C_{\epsilon 1} = 1.44, \quad C_{\epsilon 2} = 1.92. \tag{9}$$

The technical details of urbanSTREAM used in the high-resolution computational fluid dynamics simulation of urban flow, where all the buildings in the computational domain are explicitly resolved in the sense that appropriate boundary conditions are imposed at all the building surfaces (e.g.,

walls, roofs), have been described. However, the computational demands of such an approach are high and, as a consequence, sufficiently prohibitive as to preclude the simulation of flow through and above all buildings over a relatively large computational domain in a typical city environment.

In lieu of imposing correct boundary conditions on the true (but usually complex, three-dimensional) geometry of the building surfaces and fully resolving the detailed intricate flow around every individual building in a computational domain, it is convenient to consider the prediction of statistics of the mean wind and turbulence in an urban canopy that are obtained by averaging horizontally the flow properties over an area that is larger than the spacings between the individual roughness elements comprising the urban canopy, but less than the length scale over which the roughness element density changes. Towards this objective, we consider the use of a virtual building concept in urbanSTREAM whereby groups of buildings are unresolved and the aggregate of these individual buildings is treated simply as a porous medium. Here, the effects of the unresolved buildings (or, virtual buildings) on the flow are represented through a distributed mean-momentum sink in the mean momentum equation. Furthermore, additional source/sink terms in the supporting transport equations for k and ϵ are included in order to model the effects of the virtual buildings on the turbulence.

The foundations of a systematic mathematical formulation for the derivation of the governing equations for flow through an urban canopy where the individual buildings are unresolved (virtual buildings) and the aggregate of various groups of buildings (and other obstacles) is treated simply as a porous medium is described in Lien et al. [14]. Details of the implementation of this distributed drag force model can be found in Lien and Yee [15]. The representation of groups of buildings as a porous medium requires an additional modeling effort. The transport equation for the mean momentum is modified with the inclusion of a mean drag force $\bar{f}_{d,i}$ due to the effects of the virtual buildings on the flow, so

$$\frac{\partial \bar{u}_i}{\partial t} + \frac{\partial \bar{u}_j \bar{u}_i}{\partial x_j} = -\frac{\partial \bar{p}}{\partial x_i} + \nu \frac{\partial^2 \bar{u}_i}{\partial x_j^2} - \frac{\partial}{\partial x_j}(\overline{u_i' u_j'}) - 2\epsilon_{ijk}\Omega_j \bar{u}_k + \bar{f}_{d,i}, \tag{10}$$

where $\bar{f}_{d,i}$ is parameterized as follows:

$$\bar{f}_{d,i} = -\widehat{C_D}\hat{A}\left(Q\bar{u}_i + \frac{\bar{u}_j}{Q}\overline{u_i' u_j'} + \frac{\bar{u}_i k}{Q}\right), \tag{11}$$

where $\widehat{C_D}$ is the drag coefficient, $\hat{A}$ is the frontal area density (frontal area of buildings exposed to the wind per unit volume), and $Q \equiv \left(\bar{u}_i \bar{u}_i\right)^{1/2}$ is the magnitude of the (spatially-averaged) time-mean wind speed. Utilizing the eddy viscosity model for turbulent stresses of Equation (3) in Equation (11) yields the following final form for the mean drag force imposed by the virtual buildings on the flow:

$$\bar{f}_{d,i} = -\widehat{C_D}\hat{A}\left[\left(Q + \frac{5}{3}\frac{k}{Q}\right)\bar{u}_i - \nu_t\left(\frac{\partial \bar{u}_i}{\partial x_j} + \frac{\partial \bar{u}_j}{\partial x_i}\right)\frac{\bar{u}_j}{Q}\right]. \tag{12}$$

Standard turbulence models need additional modifications when applied to urban flows where buildings are treated as virtual (and represented as a distributed mean-momentum sink). Additional modifications required in the transport equations for k and ϵ were derived in Lien et al. [14] and are simply summarized here. The k- and ϵ-equations require additional source/sink terms and now take the following form:

$$\frac{\partial k}{\partial t} + \frac{\partial \bar{u}_j k}{\partial x_j} = \frac{\partial}{\partial x_j}\left[\left(\nu + \frac{\nu_t}{\sigma_k}\right)\frac{\partial k}{\partial x_j}\right] + (P_k + F) - C_{\epsilon 0}\epsilon, \tag{13}$$

and

$$\frac{\partial \epsilon}{\partial t} + \frac{\partial \bar{u}_j \epsilon}{\partial x_j} = \frac{\partial}{\partial x_j}\left[\left(\nu + \frac{\nu_t}{\sigma_\epsilon}\right)\frac{\partial \epsilon}{\partial x_j}\right] + \frac{\epsilon}{k}\Big(C_{\epsilon 1}\big(P_k + F\big) - C_{\epsilon 2}\epsilon\Big). \tag{14}$$

The term F in Equation (13) can be interpreted as an additional physical mechanism for the production/dissipation of k, and as shown in Lien et al. [14] can be approximated as

$$F = -\widehat{C_D}\hat{A}\left[\, 2Qk + \frac{1}{Q}\Big(\,\bar{u}_i\bar{u}_k\overline{u_i'u_k'}\,\Big) + \frac{3}{2Q}\Big(\,\bar{u}_k\overline{u_i'u_i'u_k'}\,\Big)\,\right], \tag{15}$$

where the triple correlation term $\overline{u_i'u_i'u_k'}$ here is modeled, following Daly and Harlow [16], as

$$\overline{u_i'u_i'u_k'} = 2C_s\frac{k}{\epsilon}\left[\,\overline{u_k'u_l'}\frac{\partial k}{\partial x_l} + \overline{u_i'u_l'}\frac{\partial \overline{u_i'u_k'}}{\partial x_l}\,\right], \tag{16}$$

where the closure constant $C_s \approx 0.3$ is used. The double correlation (turbulent stress) $\overline{u_i'u_j'}$ in Equations (15) and (16) are modeled using either the Boussinesq stress-strain relationship in Equation (3) or the explicit nonlinear stress-strain relationship in Equation (4).

3.3 Numerical framework

The coupled, nonlinear system of six partial differential equations that model the three-dimensional, highly-disturbed, building-aware turbulent flow field in the urban environment was solved numerically. The algorithm implemented in urbanSTREAM employs a fully-collocated, cell-centred storage arrangement for all transported properties. With an arbitrary, but structured, non-orthogonal finite-volume system, the mean velocity vector is decomposed into its Cartesian components to which the mean momentum equations relate. Diffusive volume-face fluxes are discretized using a second-order central differencing scheme. The higher-order quadratic upwind interpolation for convective kinematics (QUICK) scheme, described by Leonard [17], is used to approximate the convective volume-face fluxes. This second-order scheme for the discretization of the net advective flux through a control volume combines the second-order accuracy of a central differencing scheme, with the stability inherent in an upwind differencing scheme, by using in each direction separately a quadratic upstream interpolation. Furthermore, an alternative scheme is available for the approximation of the advective fluxes across a cell face; namely, the Upstream Monotonic Interpolation for

Scalar Transport (UMIST) scheme developed by Lien and Leschziner [18]. The UMIST scheme is a total variation diminishing (TVD) variant of the QUICK scheme. More specifically, the UMIST scheme generalizes QUICK by introducing a limiter to give a monotonic version of QUICK that satisfies TVD contraints.

Mass conservation is enforced indirectly by solving a pressure-correction equation which, as part of the iterative sequence, steers the pressure towards a state in which all mass residuals in the cells are negligibly small. The iterative scheme used here to enforce mass conservation is the Semi-Implicit Method for Pressure-Linked Equations (SIMPLE) described in detail by Patankar [19]. The SIMPLE algorithm provides a method for connecting the discretized forms of the mean momentum and continuity equations to give an equation linking the pressure correction at a node to its neighboring nodes. In this iterative solution sequence, $\bar{u}_i$ $(i = 1, 2, 3)$ are initially obtained with an estimated pressure field. This is continuously updated by reference to the local mass residuals, which are used to steer the pressure field towards the correct level. Within this scheme, the transport equations for $\bar{u}_i$ $(i = 1, 2, 3)$, k, and ϵ and the pressure-correction equation are solved sequentially and iterated to convergence, defined by reference to L1 residual norms for the mass and momentum components. The L1 residual norms for the mass and momentum components were normalized by the mass and momentum fluxes at the inflow plane. A convergent solution was assumed after each normalized L1 residual norm decreased below 0.001.

A fully collocated variable storage, in combination with a central differencing for pressure, is known to provoke checkerboard oscillations in the pressure field, reflecting the decoupling of the pressure and velocity fields. To avoid this, the widely used interpolation scheme proposed by Rhie and Chow [20] is used to interpolate cell-face velocities from the nodal values. This method for interpolation essentially introduces a fourth-order smoothing term based on the pressure, and prevents the occurrence of spurious pressure modes.

4.0 URBAN DISPERSION MODELS

Prediction of the highly disturbed wind field statistics using urbanSTREAM is in principle prerequisite to or co-requisite with prediction of the simpler (but nevertheless complex) problem of scalar (contaminant) dispersion within the urban environment. In particular, the prediction of turbulent flow statistics through a built-up area is required to provide the input information needed to "drive" a physically-based model for urban dispersion. Within the context of Component 1 of CRTI Project 02-0093RD, two different (but complementary) models for urban dispersion from the Eulerian perspective have been developed. Furthermore, within Component 4 of CRTI Project 02-0093RD, various three-dimensional LS trajectory models for urban dispersion have also been developed. These models for urban dispersion will be described briefly in this section.

4.1 Eulerian models for urban dispersion: urban(A)EU

The first urban dispersion model within the Eulerian framework, referred to as urbanEU, uses a source-oriented dispersion modeling technique. The model estimates dispersion of *passive* scalars within and above the urban canopy (viz., at the street and neighborhood scale). In consequence, the mean momentum equation is decoupled from the scalar transport equation, with the velocity field independent of the scalar concentration field. More specifically, the additional transport equation required for the conservation of the scalar (the contaminant) has the following form:

$$\frac{\partial C}{\partial t} + \frac{\partial \bar{u}_j C}{\partial x_j} = \frac{\partial}{\partial x_j}\left[K\frac{\partial C}{\partial x_j}\right] - \frac{\partial}{\partial x_j}\overline{u_j' c'} + Q, \tag{17}$$

where C is the mean concentration of a contaminant, K is the molecular kinematic diffusivity of the contaminant in air, Q is the source density distribution for the contaminant, and $\overline{u_j' c'}$ is the turbulent concentration (scalar) flux in the coordinate direction j (c' is the fluctuating concentration).

In Equation (17), a gradient diffusion model can be used as perhaps the simplest closure model for the turbulent concentration fluxes, although this assumption has not been rigorously justified for urban dispersion. In particular, within this popular framework the turbulent concentration fluxes are modeled as

$$\overline{u_j' c'} = -K_t \frac{\partial C}{\partial x_j}, \tag{18}$$

where K_t is the turbulent (or, eddy) kinematic diffusivity which is obtained from the turbulent viscosity ν_t (predicted by urbanSTREAM) in combination with a turbulent Schmidt number Sc_t in the following manner:

$$K_t = \frac{\nu_t}{\mathrm{Sc}_t}. \tag{19}$$

In urbanEU, we adopt this concept using a constant turbulent Schmidt number Sc_t with a value of 0.63. With the closure for the turbulent scalar fluxes given by Equations (18) and (19), the modeled transport equation for the mean concentration C reduces to the following advection-diffusion equation:

$$\frac{\partial C}{\partial t} + \frac{\partial \bar{u}_j C}{\partial x_j} = \frac{\partial}{\partial x_j}\left[\left(K + K_t\right)\frac{\partial C}{\partial x_j}\right] + Q. \tag{20}$$

In addition to using a simple gradient diffusion hypothesis to model the turbulent scalar fluxes, urbanEU also allows the option of more sophisticated closures for $\overline{u_j' c'}$. To this purpose, the tensor diffusivity model of Yoshizawa [21] has been implemented in urbanEU as an alternative closure for the turbulent scalar fluxes. This model has the following form:

$$\overline{u_j' c'} = -D_{jk} \frac{\partial C}{\partial x_k}, \tag{21}$$

where the tensor diffusivity D_{jk} is defined as

$$D_{jk} = C_{s1}\frac{k^2}{\epsilon}\delta_{jk} + C_{s2}\frac{k^3}{\epsilon^2}\left(\frac{\partial \bar{u}_j}{\partial x_k} + \frac{\partial \bar{u}_k}{\partial x_j}\right). \tag{22}$$

Here, $C_{s1} = 0.134$ and $C_{s2} = -0.032$ are two model coefficients.

In the source-oriented dispersion model implemented in urbanEU, the goal of the dispersion modeling is to calculate the mean concentration 'seen' by a detector at a given receptor location when provided the source distribution (source term) Q of the contaminant. In other words, in the source-oriented approach the advection-diffusion equation given by Equation (20) is solved forward in time for a given source distribution of contaminant $Q(\mathbf{x}, t)$ to obtain the mean concentration field $C(\mathbf{x}, t)$. Then, the concentration of contaminant 'seen' by a detector at a given receptor, denoted $\Phi(C)$, can be defined as the following integral of concentration $C(\mathbf{x}, t)$ filtered in space and time by the spatial-temporal filtering function $h(\mathbf{x}, t)$ corresponding to the response function of the detector:

$$\Phi(C) = \int C(\mathbf{x}, t)h(\mathbf{x}, t)\, d\mathbf{x}\, dt \equiv \big(C, h\big). \tag{23}$$

Therefore, this integral is simply a linear functional of C and expresses averaging of the concentration field over the spatial volume and averaging time imposed by the detector at the receptor location. This linear functional of C is defined by the inner product $\big(C, h\big)$ given in Equation (23), and allows one to calculate detector concentrations at any number of receptors located within the computational domain. However, for any new release scenario involving a different source distribution Q, the solution of Equation (20) needs to be calculated again in order to determine Φ.

Alternatively, when the detector concentration at a fixed receptor is of principal interest for a range of different emission scenarios, the alternative receptor-oriented dispersion modeling approach is useful. As a result, we have implemented a receptor-oriented dispersion model in urbanAEU, which solves the following adjoint advection-diffusion equation for the influence (or, adjunct) function C^* (with dimensional units of inverse volume):

$$-\frac{\partial C^*}{\partial t} - \frac{\partial \bar{u}_j C^*}{\partial x_j} = \frac{\partial}{\partial x_j}\left[\big(K + K_t\big)\frac{\partial C^*}{\partial x_j}\right] + h\ , \tag{24}$$

where h is the space-time filtering function of the detector at the fixed receptor location. It is important to note that Equation (24) is the adjoint of Equation (20), with C and C^* related to each other through the source function Q and detector (receptor) function h as follows:

$$\Phi(C) = \int C^*(\mathbf{x}, t)Q(\mathbf{x}, t)\, d\mathbf{x}\, dt \equiv \big(C^*, Q\big) = \big(C, h\big). \tag{25}$$

4.2 Lagrangian models for urban dispersion: urban(b)LS-(0)1

Lagrangian stochastic models for urban dispersion have also been implemented within the integrative multiscale urban modeling system. These models are described in detail in Wilson [22], and only a brief overview will be presented here. Lagrangian stochastic particle trajectory models compute forward or reverse time paths of "marked" fluid parcels released from transient or continuous sources and are "driven" using the fully three-dimensional building-resolving wind field provided by urbanSTREAM.

For the source-oriented approach within the Lagrangian description, the concentration $C(\mathbf{x}, t)$ can be determined by releasing "marked" fluid particles from the source distribution Q and following these particles forward in time using the following stochastic differential equation:

$$d\mathbf{X}(t) = \left(\mathbf{U}(t) + \nabla K_t\right) dt + \left(2K_t\right)^{1/2} d\mathbf{W}, \tag{26}$$

where $\mathbf{X}(t)$ and $\mathbf{U}(t) \equiv \mathbf{u}(\mathbf{X}(t), t)$ are the particle position and velocity at time t, respectively, and $d\mathbf{W}$ are the increments of a vector Wiener process. More specifically, "marked" fluid particles are released from the source distribution $Q(\mathbf{x}_0, t_0)$ at location $\mathbf{x}_0$ and at time t_0 and the trajectories of these particles are followed forward in time ($t > t_0$) using Equation (26). In consequence, this is a zeroth-order forward LS model (urbanLS-0) (or, random displacement model). In Equation (26), K_t is the eddy diffusivity [cf. Equations (18) and (19)]. In view of this, a zeroth-order LS particle trajectory model is formally equivalent to an eddy diffusion treatment of turbulent dispersion. In particular, Equation (26) can be interpreted as the Lagrangian description of the eddy diffusivity model given by Equation (20).[2]

A receptor-oriented version of the urbanLS-0 model given by Equation (26) can be formulated. To this purpose, we have implemented a zeroth-order backward LS model (urbanbLS-0). In the Lagrangian description, the adjunct field C^* [cf. Equation (25)] can be computed following the trajectories of marked fluid particles that are released from the receptor space-time volume h at location $\mathbf{x}_r$ and at time t_r and followed backwards in time ($t < t_r$) using the stochastic differential equation (backward Lagrangian stochastic model)

$$d\mathbf{X}(t) = \left(-\mathbf{U}(t) + \nabla K_t\right) dt + \left(2K_t\right)^{1/2} d\mathbf{W}. \tag{27}$$

It should be noted that Equation (27) is the Lagrangian equivalent of Equation (24).

It is well-known that turbulent convection cannot be represented accurately as a diffusion process unless the travel time is sufficiently long that "marked" particle position can be regarded as the outcome of a large number of random steps, in which case, by the Central Limit Theorem, particle displacement probability distributions will be Gaussian. In consequence, close to sources, the

[2]The effects of molecular diffusion embodied by the term involving K in Equation (20) is ignored in the Lagrangian description of the particle trajectories here.

diffusion treatment (which is implicit in the eddy diffusivity models described above) is incorrect, and one has a memory-dominated transport in the "near field" of the source. To account properly for this, we consider the application of a source-oriented, forward-time, first-order LS model, which explicitly models the joint evolution of the position *and velocity* of a "marked" fluid particle (urbanLS-1):

$$\begin{aligned} d\mathbf{X}(t) &= \mathbf{U}(t)\,dt, \\ d\mathbf{U}(t) &= \mathbf{a}(\mathbf{X}(t),\mathbf{U}(t),t)\,dt + \big(C_0\epsilon(\mathbf{X}(t),t)\big)^{1/2}\,d\mathbf{W}(t), \end{aligned} \tag{28}$$

where $\mathbf{X}(t)$ and $\mathbf{U}(t)$ are the (Lagrangian) position and velocity, respectively, of a "marked" fluid element (or, particle) at time t (marked by the source as the fluid element passes through it at some earlier time t'), so $(\mathbf{X},\mathbf{U})$ determines the state of the fluid particle at any time t after its intial release from the source distribution Q. In Equation (28), C_0 is the Kolmogorov "universal" constant (associated with the Kolmogorov similarity hypothesis for the form of the second-order Lagrangian velocity structure function in the inertial subrange); ϵ is the mean dissipation rate of turbulence kinetic energy; $d\mathbf{W}(t)$ are the increments of a vector-valued (three-dimensional) Wiener process; and $\mathbf{a} \equiv (a_i) = (a_1, a_2, a_3)$ is the conditional acceleration vector.

The model is fixed by the choice of a_i $(i = 1, 2, 3)$. The most important criterion for the determination of a_i is the well-mixed criterion [23] which states that an initially well-mixed distribution of particles should remain so. For Gaussian turbulence in which the (unconditional) background (Eulerian) velocity PDF has the form

$$P_E(\mathbf{u}) = \frac{1}{(2\pi)^{3/2}\big(\det\Gamma_{ij}\big)^{1/2}} \exp\left(-\frac{1}{2}\big(u_i-\overline{u}_i\big)\Gamma_{ij}^{-1}\big(u_j-\overline{u}_j\big)\right), \tag{29}$$

($\overline{u}_i$ is the mean Eulerian velocity and $\Gamma_{ij} \equiv \overline{(u_i-\overline{u}_i)(u_j-\overline{u}_j)} = \overline{u_i' u_j'}$ is the (kinematic) Reynolds stress tensor), Thomson [23] provides one particular solution for a_i that is consistent with the well-mixed criterion:

$$a_i = -\frac{1}{2}\big(C_0\epsilon\big)\Gamma_{ik}^{-1}\big(u_k-\overline{u}_k\big) + \frac{\phi_i}{P_E}, \tag{30}$$

where

$$\begin{aligned} \frac{\phi_i}{P_E} \equiv\ & \frac{1}{2}\frac{\partial\Gamma_{il}}{\partial x_l} + \frac{\partial\overline{u}_i}{\partial t} + \overline{u}_l\frac{\partial\overline{u}_i}{\partial x_l} \\ & + \left(\frac{1}{2}\Gamma_{lj}^{-1}\left[\frac{\partial\Gamma_{il}}{\partial t} + \overline{u}_m\frac{\partial\Gamma_{il}}{\partial x_m}\right] + \frac{\partial\overline{u}_i}{\partial x_j}\right)\big(u_j-\overline{u}_j\big) \\ & + \frac{1}{2}\Gamma_{lj}^{-1}\frac{\partial\Gamma_{il}}{\partial x_k}\big(u_j-\overline{u}_j\big)\big(u_k-\overline{u}_k\big). \end{aligned} \tag{31}$$

This model is general enough to allow for almost any flow complexity.

A backward-time first-order Lagrangian trajectory simulation model (urbanbLS-1), that is dual to the first-order forward-time Lagrangian trajectory simulation model given by Equation (28), can be constructed for the computation of C^* so that it exactly satisfies the duality relationship $(C, h) = (C^*, Q)$ [cf. Equation (25)]. To this end, suppose the backward-time Lagrangian trajectory model is defined as the solution to the following stochastic differential equation (with $dt' > 0$):[3]

$$\begin{aligned} d\mathbf{X}^b(t') &= \mathbf{U}^b(t')\,dt', \\ d\mathbf{U}^b(t') &= \mathbf{a}^b(\mathbf{X}^b(t'), \mathbf{U}^b(t'), t')\,dt' + \big(C_0\epsilon(\mathbf{X}^b(t'), t')\big)^{1/2}\,d\mathbf{W}(t'), \end{aligned} \tag{32}$$

where at any given time t', $(\mathbf{X}^b, \mathbf{U}^b)$ is a point in the phase space along the backward trajectory of the "marked" fluid element (here assumed to be marked or tagged as a fluid particle which at time t_r passed through the spatial volume of the detector at location $\mathbf{x}_r$).

In this receptor-oriented approach, "marked" fluid elements with final space-time coordinates $(\mathbf{x}_f, t_f)$ are sampled from a space-time density function that is proportional to the (prescribed) spatial-temporal filtering function $h(\mathbf{x}', t'|\mathbf{x}_r, t_r)$ at a receptor space-time location $(\mathbf{x}_r, t_r)$. The backward-time Lagrangian trajectories $(t' < t_f)$ of these "marked" fluid elements, which emanate from the receptor space-time volume and move towards the source (so, $t' \to t' - dt'$ with $dt' > 0$), are determined in accordance to Equation (32) and the displacement statistics of these "marked" fluid elements can be used to compute $C^*(\mathbf{x}', t'|\mathbf{x}_r, t_r)$ (which is interpreted here as a function of $\mathbf{x}'$ and t').

It can be shown [23] that for Gaussian turbulence, C^* obtained from Equation (32) for a detector with the filtering function h, and C obtained from Equation (28) for a release from the source density Q, are exactly consistent with the duality relationship $(C, h) = (C^*, Q)$ provided: (1) $\mathbf{U}^b$ in Equation (32) is related to $\mathbf{U}$ in Equation (28) as $\mathbf{U}^b(t) = \mathbf{U}(t)$; and, (2) $\mathbf{a}^b$ in Equation (32) is related to $\mathbf{a}$ in Equation (28) as

$$a_i^b(\mathbf{x}, \mathbf{u}, t) = a_i(\mathbf{x}, \mathbf{u}, t) - C_0\epsilon(\mathbf{x}, t)\frac{\partial}{\partial u_i}\ln P_E(\mathbf{u}). \tag{33}$$

Substituting Equations (29) and (30) in Equation (33), an explicit form for a_i^b (valid for Gaussian turbulence) can be obtained as

$$a_i^b = \frac{1}{2}\big(C_0\epsilon\big)\Gamma_{ik}^{-1}\big(u_k - \overline{u}_k\big) + \frac{\phi_i}{P_E}. \tag{34}$$

Note that a_i^b differs from a_i by virtue of a sign change on the first term (or, "fading" memory term) on the right-hand-side of Equation (33). The second term ("drift" term due to spatial inhomogeneity and/or temporal non-stationarity in the velocity statistics of the turbulent flow) on the right remains invariant under a time reversal operation.

[3]Here, $d\mathbf{X}^b(t') \equiv \mathbf{X}^b(t') - \mathbf{X}^b(t' - dt')$ and $d\mathbf{U}^b(t') \equiv \mathbf{U}^b(t') - \mathbf{U}^b(t' - dt')$ with $dt' > 0$.

5.0 MODEL VALIDATION

In this section, the predictive capabilities of the urban flow and dispersion models are validated against very detailed and comprehensive water channel and full-scale data sets for dispersion in an urban area. More specifically, the predictive capabilities of urbanSTREAM and urban(A)EU for urban dispersion predictions are illustrated.

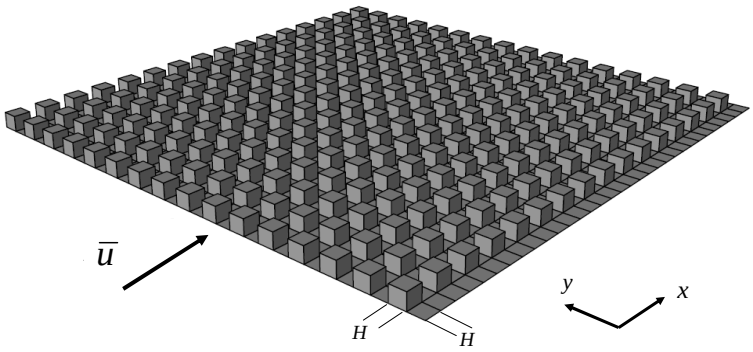

Figure 6: A three-dimensional perspective view showing the geometry of the regular and aligned array of cubes and the Cartesian coordinate system used. Here, x is in the streamwise direction and y is in the spanwise direction.

5.1 Application to idealized obstacle array

First, we evaluate the model performance of urbanSTREAM/urban(A)EU by presenting a detailed comparison between the results of a numerical simulation with measurements of urban dispersion obtained in a water-channel experiment. The water-channel experiment is fully described in Hilderman and Chong [24], and the reader is referred to this report for the relevant details of the experiment.

The water channel experiment simulated a neutrally-stratified atmospheric boundary-layer flow over a regular array of three-dimensional (3-D) buildings. A schematic drawing of the 3-D building array is shown in Figure 6. The array consists of sharp-edged cubes with a characteristic dimension $L = W = H = 31.75$ mm, where L, W and H are the length, width and height of the obstacles. A total of 256 cubes was placed in an aligned array consisting of 16 rows of 16 cubes. The array filled the entire spanwise dimension (width) of the water channel. The streamwise and spanwise face-to-face spacings between cubes was H giving frontal and plan area indices (λ_f and λ_p, respectively)

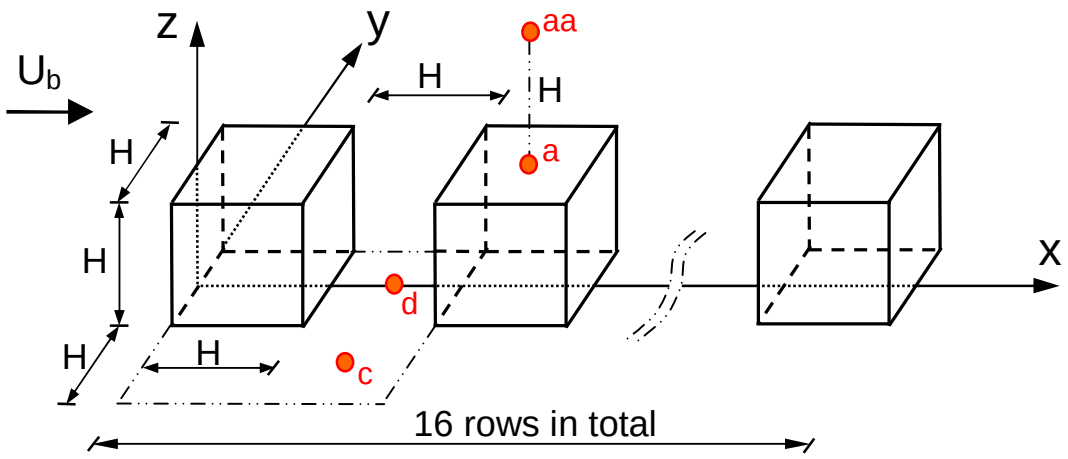

Figure 7: Geometry of the regular and aligned array of cubes in the water channel depicting the eighth column of the obstacles. The location of the ground-level source is marked by d. U_b is the mean streamwise velocity at the top of the rough-walled boundary layer.

of 0.25.[4]

For the water channel simulations of dispersion in the obstacle array, a ground-level point source consisting of a vertical stainless steel tube (2.8 mm I.D. and 3.1 mm O.D.) was used, with the outlet of the tube placed just above the wire mesh that served as the ground roughness elements. The source emitted a sodium fluorescein dye tracer at a constant flow rate of 12×10^{-3} l min^{-1} with low discharge momentum (weak vertical jet). The source was located between the first and second rows of obstacles in the spanwise-oriented street canyon at a position lying at the intersection of the first row and eighth column of obstacles (where the rows are numbered in increasing order in the streamwise direction from the leading (windward) edge of the array and the columns are numbered in increasing order in the spanwise direction from the right-hand side of the array when looking in the flow direction – see Figure 6). This source location will be referred to as location d as shown in Figure 7. The instantaneous concentration field in the dispersing dye plume was measured using the laser-induced fluorescence (LIF) technique.

For the simulations to be reported, the model domain used to simulate the flow within and over the 3-D building array spanned $-15 \leq x/H \leq 46$ with the windward face of the first row of cubes placed at $x/H = 0$. The spanwise extent of the domain was $18H$ (spanning 9 columns of cubes in the spanwise direction with $-9 \leq y/H \leq 9$) and the domain height was $11H$ ($0 \leq z/H \leq 11$), where z

[4]The frontal area index of an obstacle array is defined as $\lambda_f \equiv A_f/A_L$, where A_f is the frontal (windward) area of an obstacle and A_L is the lot area (surface area within which a single obstacle sits in the array). The plan area index is defined as $\lambda_p = A_p/A_L$, where A_p is the plan (floor) area of the obstacle.

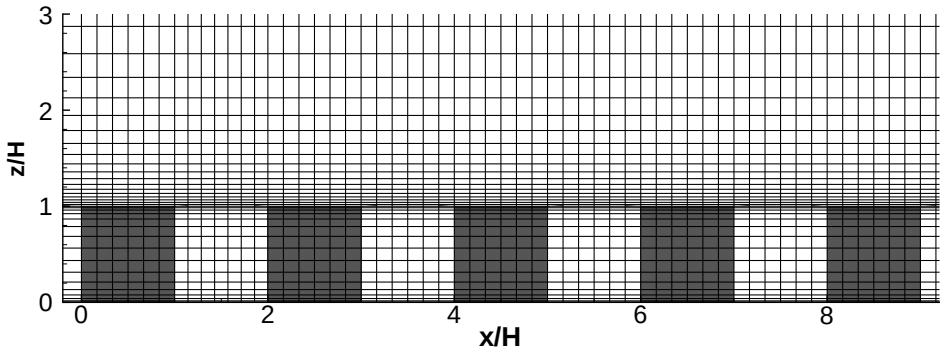

Figure 8: A partial x-z view at $y = 0$ of the computational grid used for the prediction of flow over the aligned array of cubes.

is the vertical coordinate direction measured from ground level. The domain height was sufficiently deep to provide an appropriate computational domain within which the flow changes near the surface can occur without being moulded by the boundary conditions (i.e., free slip conditions) imposed at the outer boundary layer.

The discretization of the computational domain is displayed in Figure 8. A non-uniform coarse grid of $228 \times 111 \times 48$ control volumes (in the streamwise, spanwise and vertical directions, respectively) was used for the discretization of the computational domain. As shown in Figure 8, the grid lines were preferentially concentrated in the vicinity of the ground and rooftops, where the gradients in the flow properties are expected to be greatest. The spacing between the grid lines was gently stretched with increasing distance from these surface in the vertical (z-) direction. The grid spacing was uniform in the horizontal (x- and y-) directions.

Figure 9 displays predictions for crosswind profiles of the mean concentration C (normalized by the source concentration C_s) at half-canopy height ($z/H = 0.5$) at five alongwind locations $(x - x_s)/H$, where $x_s = 1.5H$ is the streamwise location of the ground-level source (cf. Figure 7). The corresponding experimental measurements (open circles) are also shown in the figure for comparison. In general, the predictions for the mean concentration show good agreement with the measurements at all the locations, although they are seen to over-predict slightly the mean-plume centreline concentration (at $y/H = 0$), especially further from the source. Furthermore, the peak mean concentration is over-predicted by as much as about 20% at the farthest downwind station. Note that the model under-predicts the crosswind spread of the plume at alongwind locations further from the source (i.e., for $(x - x_s)/H \gtrsim 6$), which is consistent with the slight over-prediction of the mean concentration at these locations. Nevertheless, it can be inferred from the results of Figure 9 that the horizontal spread rate of the mean plume and the rate of decay of the mean-plume centreline concentration, as a function of downwind distance from the source, is predicted

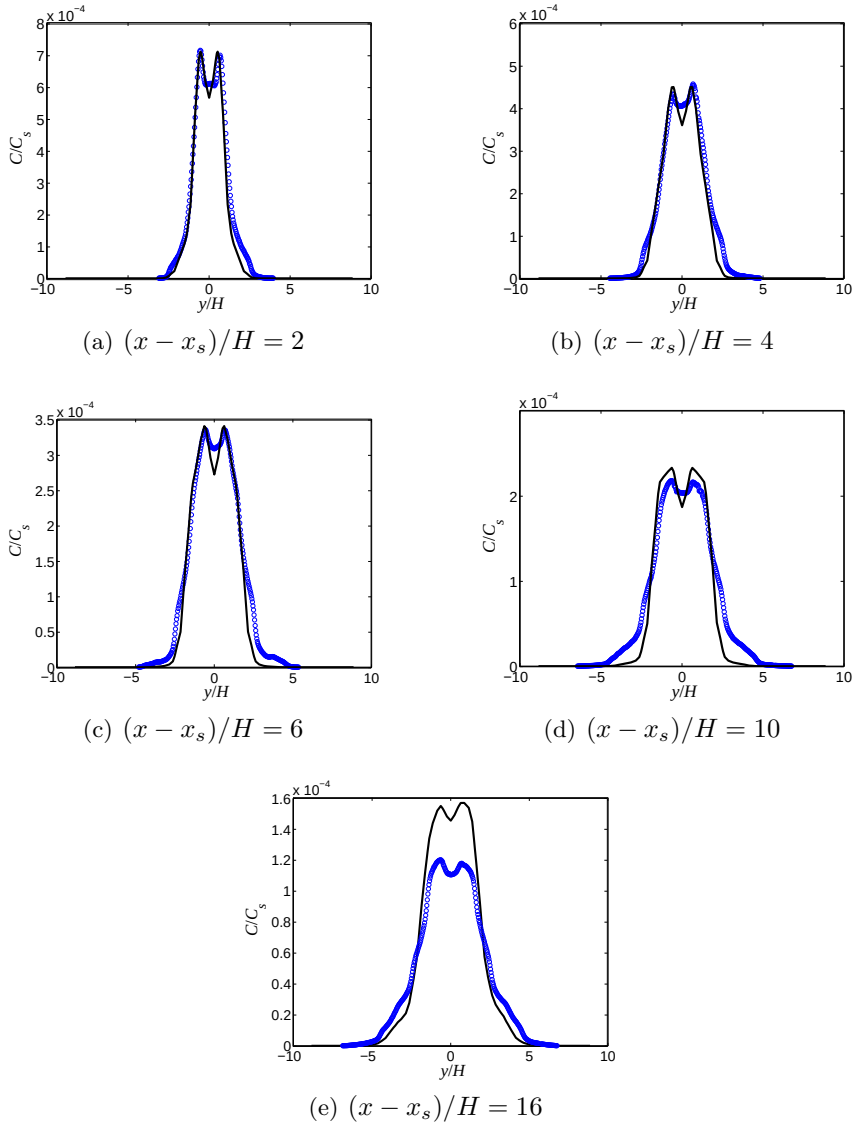

(a) $(x - x_s)/H = 2$ (b) $(x - x_s)/H = 4$

(c) $(x - x_s)/H = 6$ (d) $(x - x_s)/H = 10$

(e) $(x - x_s)/H = 16$

Figure 9: Crosswind profile of the normalized mean concentration, C/C_s, measured at various alongwind positions at half-canopy height ($z/H = 0.5$). The plot also includes a model prediction for the normalized mean concentration (solid line). Here, C_s is the source concentration and $x_s = 1.5H$ is the streamwise location of the ground-level source.

quite well by the model.

It is seen from Figure 9 that the shapes of the mean concentration profiles are correctly predicted

by the model. In particular, the model correctly predicts the non-Gaussian distribution of the crosswind mean concentration profile, which is seen to exhibit a distinctly bimodal form. This bimodel form in the crosswind mean concentration profile is probably due to the bifurcation of the plume as the material is swept around an obstacle on either side of its wake. Note that the crosswind location of these two modes in the mean concentration profile is in good conformance with the measurements. In addition, ratio of the peak value to the centreline value in the mean concentration is generally predicted well by the model over the downwind range of the concentration data. Finally, the crosswind locations y_p of the mean concentration peaks evolve slowly with $(x - x_s)/H$, increasing from $|y_p|/H \approx 0.5$ near the source at $(x - x_s)/H = 2$ to ≈ 0.85 at the farthest station at $(x - x_s)/H = 16$. This observed evolution of y_p in the streamwise direction is captured properly by the model predictions.

5.2 Application to Joint Urban 2003 field experiment

Here, a computational study is performed in which the capabilities of urbanSTREAM and urban(A)EU for urban dispersion predictions are examined by reference to a full-scale experimental study of flow and dispersion in a real cityscape (Oklahoma City, Oklahoma). Joint Urban 2003 (JU2003) experiment was a major urban study that was conducted in Oklahoma City, Oklahoma during the period from June 28 to July 31, 2003 [25]. The principal objective of JU2003 was to obtain high-quality meteorological and tracer data sets documenting urban flow and dispersion in a real city on a range of scales: namely, from flow and dispersion in and around a single city block (street canyon at building scale), to that in and around several blocks in the central business district (CBD) of downtown Oklahoma City (neigborhood scale), and finally to that in the suburban area several kilometers from downtown Oklahoma City (urban scale).

Some capabilities of the modeling system are presented with the aid of numerical simulations performed for a built-up (urban) region in Oklahoma City, Oklahoma. The modeling domain with the extent of $1,934.25$ m $\times$ $3,610.6$ m $\times$ 800.0 m in the x- (or, W-E), y- (or, S-N) and z- (or, vertical) directions, respectively, covers the CBD of Oklahoma City and surrounding environs. At ground level where $z = 0$, the southwest corner of the modeling domain (see Figure 10) is at the following coordinates in the Universal Transverse Mercator (UTM) coordinate system[5]: zone = 14, $x_0 = 633,683$ UTM easting and $y_0 = 3,923,940$ UTM northing (or, equivalently, in the geodetic coordinate system this location is 35.449959° N and -97.52694° E). The internal coordinate system used in urbanSTREAM is shown in Figure 10, where the southwest corner of the modeling region is chosen as the origin $(0, 0)$ in the x-y (horizontal) plane. All distances shown here have been normalized by a reference length scale which is chosen in this case to be $\Lambda_{\text{ref}} = 644.75$ m. Hence, in this internal coordinate system, the northeast corner of the modeling region is referenced as $(3, 5.6)$. A proper subset within this modeling region is chosen as the region in which buildings will be explicitly resolved in the flow simulation; for this example, this rectangular building-aware region

[5]The UTM easting coordinate reported here and elsewhere in this report is referenced relative to the central meridian of the zone.

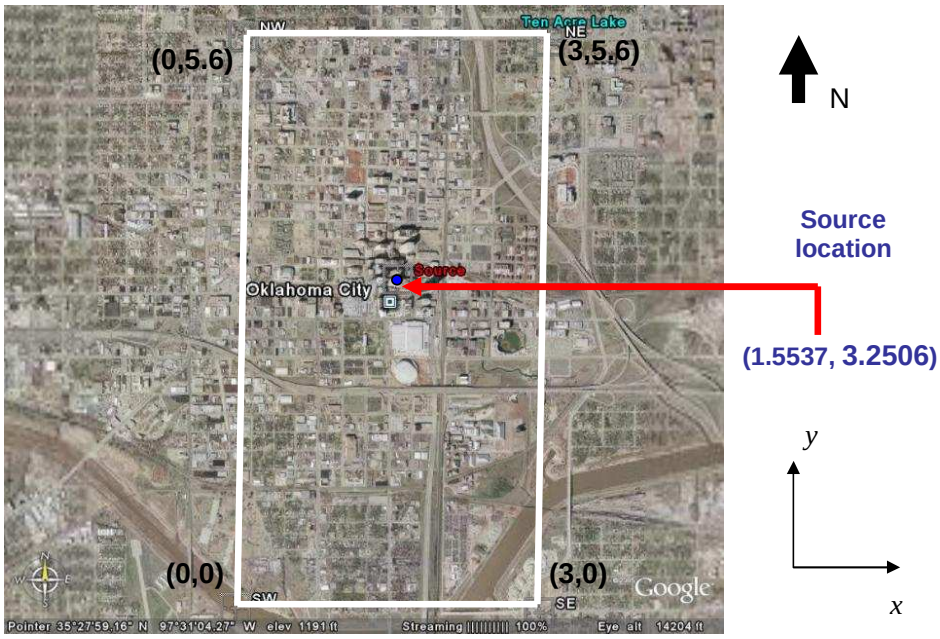

Figure 10: Computational domain used for simulation of flow and dispersion in Oklahoma City.

(644.75 m $\times$ 709.23 m) has its southwest corner at $(1, 2.5)$ and its northeast corner at $(2, 3.6)$. In the portion of the modeling region lying outside the building-aware region, all buildings are treated as virtual and their effects on the flow are modeled using a distributed drag force representation in the mean momentum equations.

ESRI Shapefiles of the shapes, locations and heights of buildings in Oklahoma City are available from the Joint Urban 2003 archival database (https://ju2003-dpd.dpg.army.mil). These Shapefiles were used in urbanGRID to generate automatically a grid mesh over the modeling region as shown in Figure 11. The simulation was carried out in a three-dimensional Cartesian framework, and curved surfaces on buildings or planar building surfaces that are not aligned with the grid lines are approximated by stepwise surfaces. A mesh of $99 \times 139 \times 69$ grid lines in the x-, y-, and z-directions, respectively, was used to accomodate all the necessary geometrical details. The interior building-aware region was covered with a fine calculation grid of $55 \times 100 \times 69$ grid lines to better approximate the building features in this region. The grid arrangement adopted here is shown in the x-y plane in Figure 11. Hence, the fine grid used for the building-aware region contains 379,500 nodes, whereas the entire computational domain was covered with a mesh of 945,509 nodes. The grid lines were preferentially concentrated near the solid surfaces (ground, building rooftops and walls) where the gradients in the flow properties are expected to be greatest, and the spacing between the grid lines was gently stretched with increasing distance from the solid surfaces.

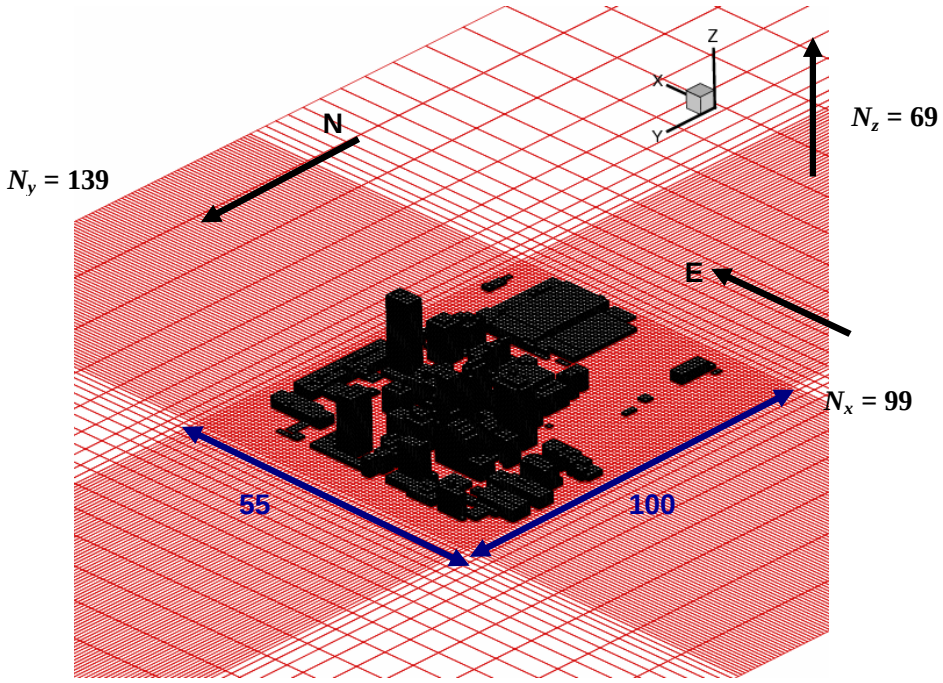

Figure 11: Computational grid generated by urbanGRID for Oklahoma City.

The flow field statistics predicted by urbanSTREAM was obtained and these wind statistics were used to "drive" an urban dispersion model in both the source-oriented (urbanEU) and receptor-oriented (urbanAEU) modes within the Eulerian framework. Furthermore, these wind field statistics were also used to "drive" a first-order Lagrangian stochastic model for urban dispersion (urbanLS, or more precisely urbanLS-1). The simulations were conducted for the second continuous 30-min release of sulfer hexafluoride (SF_6) in Intensive Observation Period-9 (IOP-9), which occurred in the period from 06:00–06:30 UTC (01:00–01:30 CDT) on 28 July 2003. The SF_6 tracer gas was released at a point from a specially designed gas dissemination system that included a mass flow controller attached to a Campbell Scientific CR-23 data logger [26]. The dissemination point was located on the south side of Park Avenue (latitude 35.4687° N; longitude −97.5156° E) with a release height of 1.9 m. This source location was near the center of the computational domain (see Figure 10). The constant gas release rate for this experiment was 2.0 g s^{-1}.

The SF_6 plume concentrations were measured using Programmable Integrating Gas Samplers (PIGS) deployed by National Atmospheric and Oceanic Administration (NOAA) Atmospheric Research Laboratory Field Research Division (ARLFRD). The subsequent analysis of the samples was performed using an Automated Tracer Gas Analysis System (ATGAS) which used gas chromatography (GC) analysis techniques along with autosampler capabilities to give time-integrated

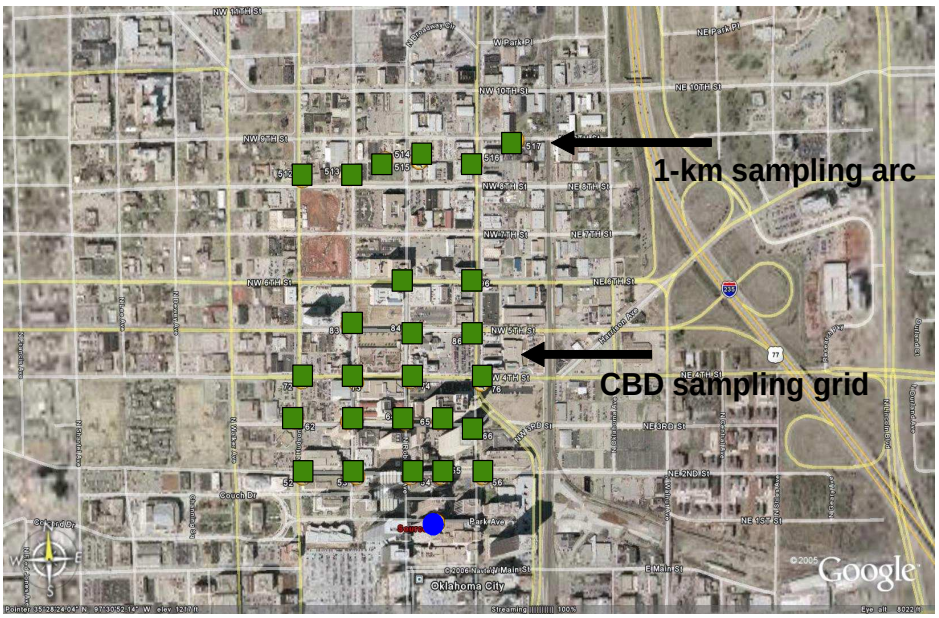

Figure 12: Detectors (squares) were positioned in the CBD sampling grid and at the 1-km sampling arc for measurement of the time-averaged tracer concentrations released from the indicated source (solid circle).

concentration measurements. The sampling system was designed to provide average SF_6 plume concentrations over specific time intervals at given receptor locations. The PIGS collected 12 samples by pumping air into 12 individual Tedlar bags. Subsequently, the bag samples were analyzed using the ATGAS. The grid of sampling stations at which predictions of SF_6 plume concentrations were compared with measurements is shown in Figure 12 in relationship to the location of the source. The samplers used for comparison include 19 samplers located on the CBD sampling grid and six samplers located along the 1-km sampling arc.

Figure 13 compares predictions of the mean concentration [in parts-per-trillion by volume (pptv)] obtained using urbanEU, urbanAEU and urbanLS-1 with the experimental concentration data measured at 10 different sampling locations along Kerr Avenue and McGee Avenue. Similarly, Figure 14 shows comparisons of mean concentration obtained using the three dispersion models with experimental concentration measurements made at eight sampling stations located along 4th Street and 5th Street. Finally, Figure 15 exhibits predicted and observed mean concentration obtained at two sampling locations along 6th Street and six sampling stations along the 1-km sampling arc. The experimental concentration data shown here is for a 30-min averaging time.

Generally speaking, the predictions for mean concentration at or near the mean plume centerline

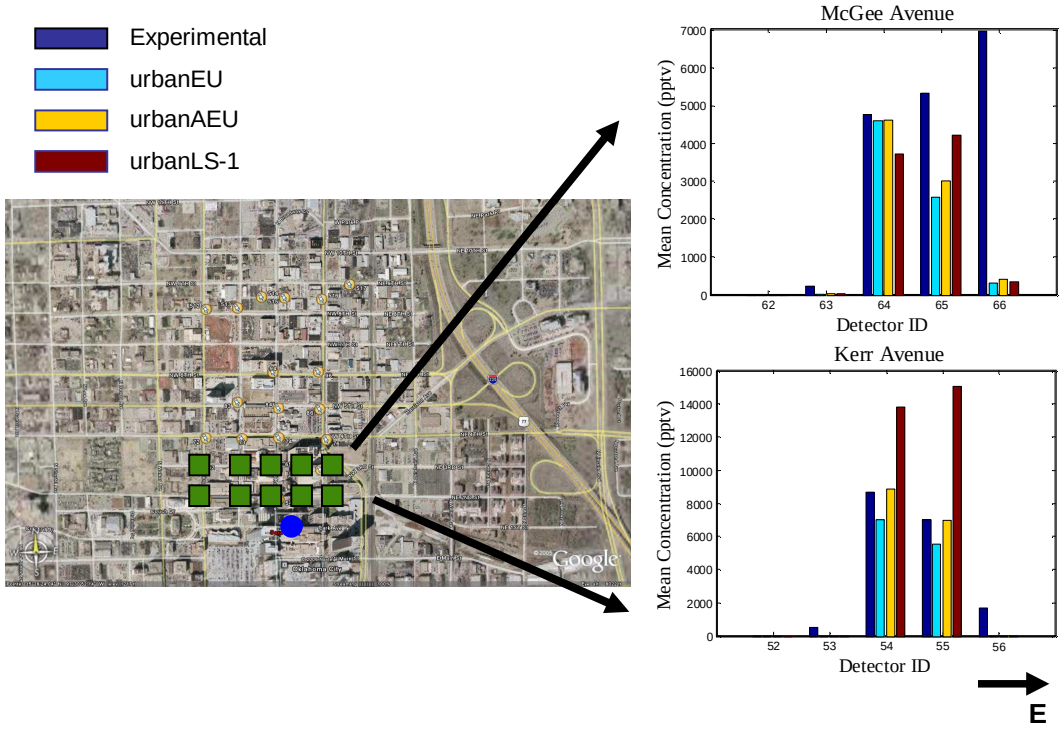

Figure 13: Comparison of predicted mean concentrations obtained from urbanEU, urbanAEU and urbanLS-1 with experimental measurements obtained with detectors along Kerr Avenue and McGee Avenue.

were quite good, with predictions within a factor of two of the observed concentration. However, the predicted concentrations at sampling locations 56, 66, and 76 were more than a factor of five lower than the experimentally measured values, suggesting that either the predicted plume was too narrow or the eastern edge of the predicted plume was too far west at these locations. Furthermore, it is interesting to note that the 30-min average concentration at the receptor calculated using the influence function (receptor-oriented approach) generally agrees well with the concentration predicted using the source-oriented approach. The discrepancy in the predictions using these two approaches is due to the non-uniform grid utilized in the simulations (the mesh was finer in the region surrounding the source and coarser generally in the region downwind of the source where the receptors were located).

6.0 CONCLUSIONS

This paper provides a general overview of the major components of the integrative multiscale urban modeling system developed under CRTI Project 02-0093RD. The principal objective is the

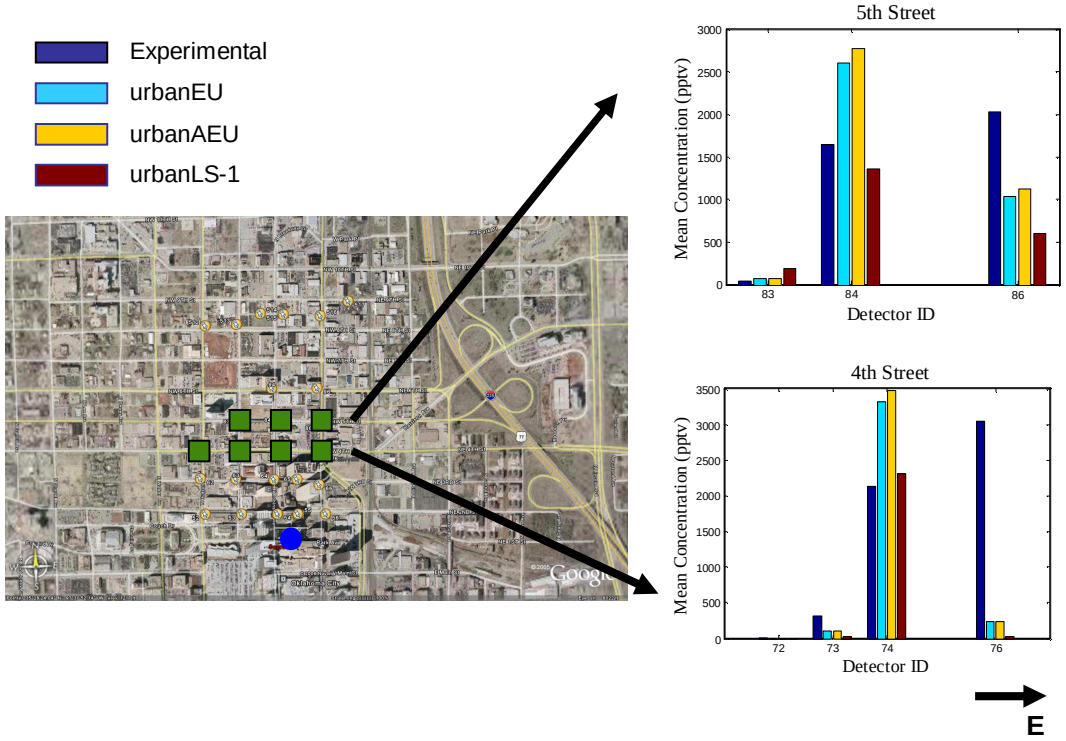

Figure 14: Comparison of predicted mean concentrations obtained from urbanEU, urbanAEU and urbanLS-1 with experimental measurements obtained with detectors along 4th Street and 5th Street.

development of an advanced, fully validated, state-of-the-science modeling system for the prediction of urban flow (i.e., turbulent flow through cities) and the concomitant problem of modeling the dispersion of CBRN agents released in a populated urban complex. The current configuration of the prototype integrative multiscale urban modeling system is shown in Figure 16. The configuration has been implemented in the computational infrastructure at Environmental Emergency Response Section (EERS) at Canadian Meteorological Centre.

The multiscale urban modeling system exhibited in Figure 16 involves the representation of multiple scales of motion, from the mesoscale to the building scale. This representation is realized in terms of a nested set of flow and dispersion models. On the largest (regional) scale, an operational version of GEM at 15-km resolution provides the initial and lateral boundary conditions for a cascade of finer-resolution flow models. These include the "urbanized" GEM LAM flow models that have been configured to operate on three computational grids nested within the regional domain used by GEM. The urbanized GEM LAM at 2.5-km resolution provides the initial and lateral boundary conditions to drive a finer-resolution GEM LAM simulation at 1.0-km resolution; and, the latter simulation

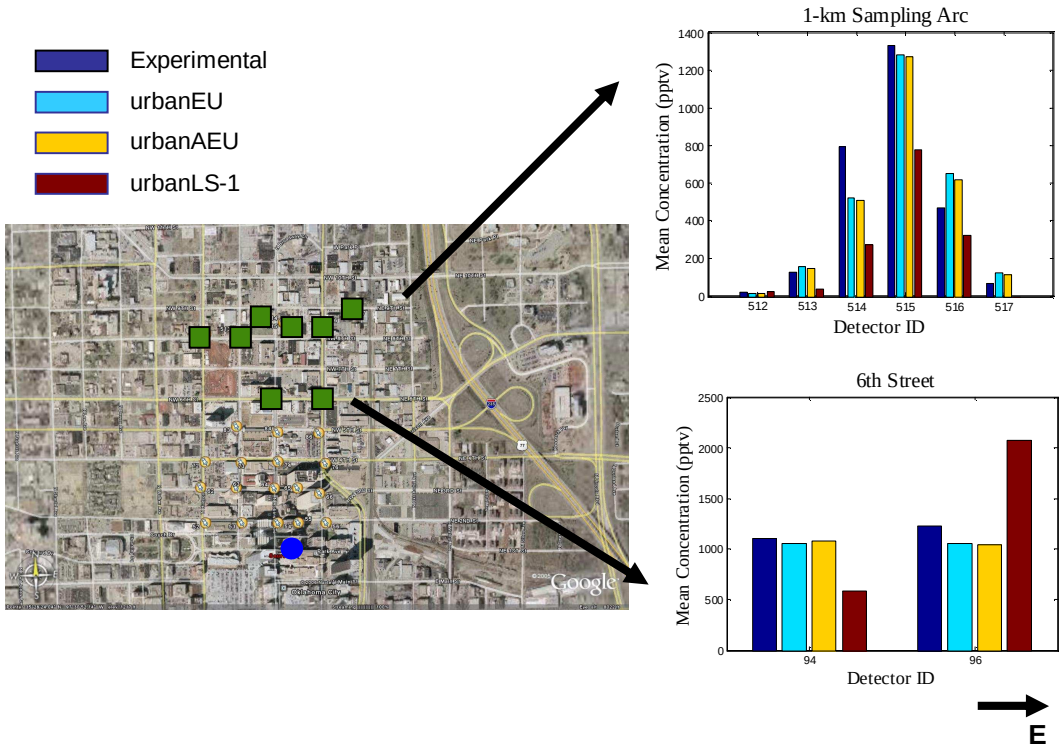

Figure 15: Comparison of predicted mean concentrations obtained from urbanEU, urbanAEU and urbanLS-1 with experimental measurements obtained with detectors along 6th Street and the 1-km sampling arc.

provides the initial and lateral boundary conditions that drive a still finer-resolution GEM LAM simulation at 250-m resolution. This information is used to provide the inflow boundary conditions required for the highest-resolution building-aware urban flow model (urbanSTREAM) that provides predictions of the detailed flow at the building scale (typically 2–5 m resolution). The detailed wind statistics, provided by the flow models over an urban area, are used as input to the urban dispersion models; namely, urban(A)EU and urban(b)LS which are based, respectively, on an Eulerian and Lagrangian description of the dispersion.

The next step is to transition this prototype of an integrative multiscale urban modeling system towards the status of an operational system is functional at a government operations facility. The integrated modeling system will provide potentially a key-enabling technology that can serve as a primary national reach-back and support centre for CBRN planning, real-time assessment, and emergency response. To achieve this objective, future effort will need to be focused on three major areas: namely, (1) advanced modeling capability; (2) infrastructure for the development of supporting data and tools required for the operational system; and (3) demonstration of the

operational system.

The first area of future work will involve providing significant improvements to the prototype system exhibited in Figure 16. This effort should be focused on the following areas: improvements to the urban parameterization scheme in the mesoscale model; incorporation of thermal effects in the building-resolving CFD model; coupling of this capability with the thermal effects as parameterized in the "urbanized" mesoscale flow model; inclusion of facility for prediction of dense gas dispersion in an urban environment; and, development of techniques for the fusion of CBRN sensor data with model predictions for source reconstruction. With respect to source reconstruction, it should perhaps be noted that significant progress has already been made. In particular, a Bayesian inferential methodology used in conjuction with the adjoint (receptor-oriented) method for representation of the source-receptor relationship was described by Yee [27–29], Yee et al. [30], Keats et al. [31, 32] and Yee [33] for the determination of source parameters for dispersion of conservative and non-conservative scalars in simple (level, unobstructed terrain) and complex (e.g., urban terrain, complex terrain on continental scales) environments.

The second area of future effort concerns the acquisition and development of the datasets and functionalities required to transition the prototype modeling system to a fully operational demonstration status. This requires provision of supporting databases such as urban building and morphology data over all major Canadian cities, databases of population distribution, hazard material source characteristics for various CBRN release modes (e.g., improvised dispersion devices, sprayers, etc.), and CBRN material and toxicological properties. This effort should also involve providing computational efficiency enhancements of the CFD model through parallel algorithm development, and full integration of the resulting modeling system into the computational and communications infrastructure within the government operations facility.

The third area of future effort involves demonstrating and exercising the operational system for a number of CBRN scenarios in various major Canadian cities, including participation in various national-to-local exercises (e.g., support of Vancouver Winter Olympics) and improving the modeling system products through user feedback from the first-responder community.

The full implementation of the proposed advanced modeling capability will provide unique CBRN operational tools and services that will be readily accessible by first responders. In particular, such a system can be used to provide near real-time Canadian city-specific predictions of airborne plumes resulting from hazardous releases of CBRN and/or toxic industrial materials. These decision support products can be used: (1) for pre-planning and as training aids for first responders; (2) to guide forensics analysis by providing comprehensive post-event reconstruction of a purported CBRN agent release; (3) to provide optimal placement of a limited number of CBRN sensors in a city; (4) to guide the planning of safe evacuation routes; and, (5) to provide estimates of risks associated with certain courses of action and to select the most appropriate emergency response strategy. The

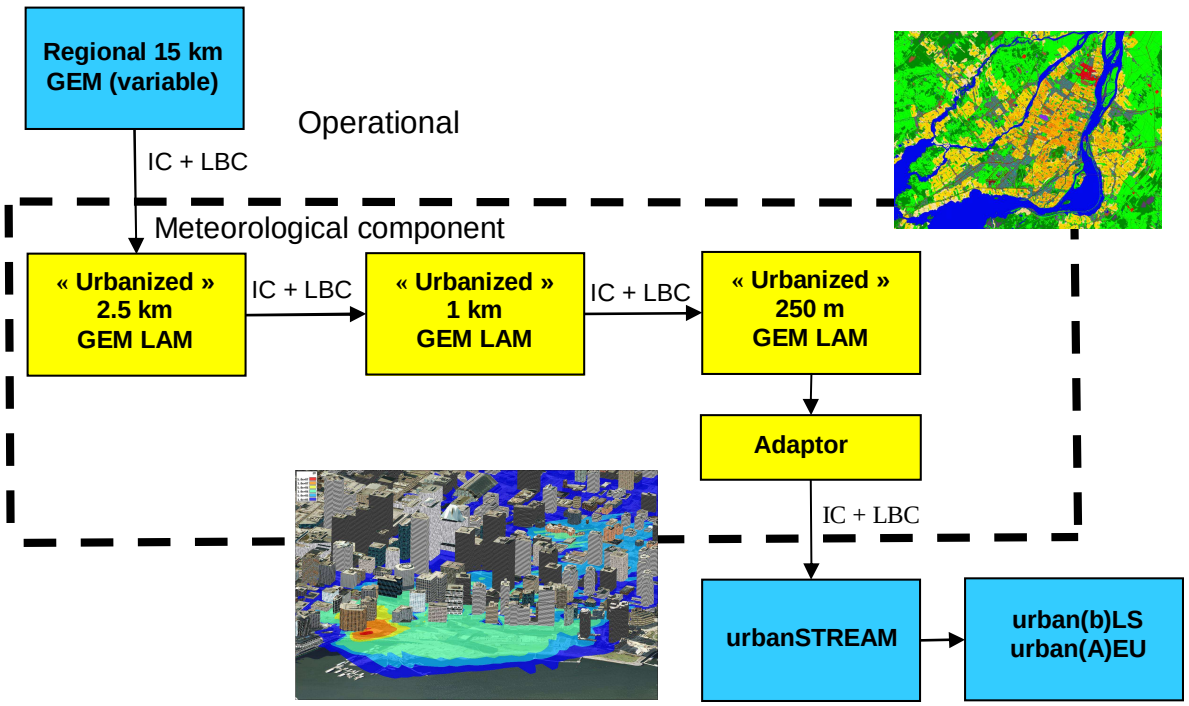

Figure 16: A prototype of the integrative multiscale urban modeling system that is currently undergoing testing at Canadian Meteorological Centre.

development of this high-fidelity, multiscale and multi-physics modeling system and its realization as a fully functional operational system in a government operations facility will provide a unique real-time modeling and simulation tool for prediction of injuries, casualties, and contamination required to support Canada's more broadly based efforts at advancing counter-terrorism planning and operational capabilities against CBRN threats for both domestic and international operations.

Acknowledgements The authors wish to acknowledge support from the Chemical Biological Radiological Nuclear Research and Technology Initiative (CRTI) Program under project number CRTI-02-0093RD.

7.0 REFERENCES

[1]. United States Government Accountability Office (2008). *First Responders' Ability to Detect and Model Hazardous Releases in Urban Areas Is Significantly Limited.* http://www.gao.gov/new.items/d08180.pdf.

[2]. Côté, J., Gravel, S., Méthot, A., Patoine, A., Roch, M. and Staniforth, A. (1998). *The Operational CMC-MRB Global Environmental Multiscale (GEM) Model. Part I: Design Considerations and Formulation.* Monthly Weather Review, 126, 1373–1395.

[3]. Côté, J., Desmarais, J.-G., Gravel, S., Méthot, A., Patoine, A., Roch, M. and Staniforth, A. (1998). *The Operational CMC-MRB Global Environmental Multiscale (GEM) Model. Part II: Results.* Monthly Weather Review, 126, 1397–1418.

[4]. Côté, J., Roch, M., Staniforth, A. and Fillion, L. (1993). *A Variable-Resolution Semi-Lagrangian Finite-Element Global Model of the Shallow Water Equations.* Monthly Weather Review, 121, 231–243.

[5]. Mailhot, J., Sarrazin, R., Bilodeau, B., Brunet, N. and Pellerin, G. (1997). *Development of the 35-km Version of the Operational Regional Forecast System.* Atmos-Ocean, 35, 1–28.

[6]. Masson, V. (2000). *A Physically-Based Scheme for the Urban Energy Budget in Atmospheric Models.* Boundary-Layer Meteorol., 94, 357–397.

[7]. Masson, V., Grimmond, C. S. B. and Oke, T. R. (2002). *Evaluation of the Town Energy Balance (TEB) Scheme with Direct Measurements from Two Districts in Two Cities.* J. Appl. Meteorol., 41, 1011–1026.

[8]. Lemonsu, A., Leroux, A., Bélair, S., Trudel, S. and Mailhot, J. (2006). *Methodology of Urban Cover Classification for Atmospheric Modeling.* Preprints, Sixth Symposium on the Urban Environment, 30 January–2 February 2006, Atlanta, GA, American Meteorological Society, Paper 5.5.

[9]. Yee, E., Lien, F.-S. and Ji, H. (2007). *Technical Description of Urban Microscale Modeling System: Component 1 of CRTI Project 02-0093RD.* DRDC Suffield TR 2007–067, Defence R&D Canada – Suffield, Ralston, Alberta.

[10]. ESRI (1998). *ESRI Shapefile Technical Description: An ESRI White Paper.* ESRI, 380 New York Street, Redlands California, USA.

[11]. Warmerdam, F. (1998). *Shapelib C Library V1.2.* http://shapelib.maptools.org.

[12]. Speziale, C. G. (1987). *On Nonlinear k-l and k-ϵ Models of Turbulence.* J. Fluid Mech., 178, 459–475.

[13]. Launder, B. E. and Spalding, D. B. (1974). *The Numerical Computation of Turbulent Flows.* Comp. Meth. Appl. Mech. Eng., 3, 1112–1128.

[14]. Lien, F.-S., Yee, E. and Wilson, J. D. (2005). *Numerical Modeling of the Turbulent Flow Developing Within and Over a 3-D Building Array, Part II: A Mathematical Foundation for a Distributed Drag Force Approach.* Boundary-Layer Meteorol., 114, 245–285.

[15]. Lien, F.-S. and Yee, E. (2005). *Numerical Modeling of the Turbulent Flow Developing Within and Over a 3-D Building Array, Part III: A Distributed Drag Force Approach, Its Implementation and Application.* Boundary-Layer Meteorol., 114, 287–313.

[16]. Daly, B. J. and Harlow, F. H. (1970). *Transport Equations of Turbulence.* Phys. Fluids, 13, 2634–2649.

17]. Leonard, B. P. (1979). *A Stable and Accurate Convective Modeling Procedure Based on Quadratic Upstream Interpolation.* Comp. Meth. Appl. Mech. Eng., 19, 59–98.

[18]. Lien, F.-S. and Leschziner, M. A. (1994). *Upstream Monotonic Interpolation for Scalar Transport with Applications to Complex Turbulent Flows.* Int. J. Numer. Methods Fluids, 19, 527–548.

[19]. Patankar, S. V. (1980). *Numerical Heat Transfer and Fluid Flow.* New York: Hemisphere Publishing Corporation.

[20]. Rhie, C. M. and Chow, W. L. (1983). *Numerical Study of the Turbulent Flow Past an Airfoil With Trailing Edge Separation.* AIAA J., 21, 1525–1532.

[21]. Yoshizawa, A. (1985). *Statistical Analysis of the Anisotropy of Scalar Diffusion in Turbulent Shear Flows.* Phys. Fluids, 28, 3226–3231.

[22]. Wilson, J. D. (2007). *Technical Description of Urban Microscale Modeling System: Component 4 of CRTI Project 02-0093RD.* J. D. Wilson and Associates, Edmonton, Alberta.

[23]. Thomson, D. J. (1987). *Criteria for the Selection of Stochastic Models of Particle Trajectories in Turbulent Flows.* J. Fluid Mech., 180, 529–556.

[24]. Hilderman, T. and Chong, R. (2007). *A Laboratory Study of Momentum and Passive Scalar Transport and Diffusion Within and Above a Model Urban Canopy.* DRDC Suffield CR 2008-025, Defence R&D Canada – Suffield, Ralston, Alberta.

[25]. Allwine, K. J., Leach, M. J., Stockham, L. W., Shinn, J. S., Hosker, R. P., Bowers, J. F. and Pace, J. C. (2004). *Overview of Joint Urban 2003 – An Atmospheric Dispersion Study in Oklahoma City.* Symposium on Planning, Nowcasting, and Forecasting in the Urban Zone. Seattle, Washington: American Meteorological Society.

[26]. Clawson, K. L., Carter, R. G., Lacroix, D. J., Hukari, N. F. and Allwine, K. J. (2004). *Joint Urban 2003 Vertical SF_6 Real-Time Analyzer and Time-Integrated Sampler Data Characteristics*. Fifth Conference on Urban Environment, Vancouver, British Columbia, American Meteorological Society.

[27]. Yee, E. (2005). *Probabilistic Inference: An Application to the Inverse Problem of Source Function Estimation*. The Technical Cooperation Program (TTCP) Chemical and Biological Defence (CBD) Group Technical Panel 9 (TP-9) Annual Meeting, Defence Science and Technology Organization, Melbourne, Australia.

[28]. Yee, E. (2006). *A Bayesian Approach for Reconstruction of the Characteristics of a Localized Pollutant Source from a Small Number of Concentration Measurements Obtained by Spatially Distributed "Electronic Noses"*. Russian-Canadian Workshop on Modeling of Atmospheric Dispersion of Weapon Agents, Karpov Institute of Physical Chemistry, Moscow, Russia.

[29]. Yee, E. (2007). *Bayesian Probabilistic Approach for Inverse Source Determination from Limited and Noisy Chemical or Biological Sensor Concentration Measurements*. Chemical and Biological Sensing VIII (Augustus W. Fountain III, ed), Proc of SPIE Vol. 6554, 65540W, doi:10.1117/12.721630, 12 pp.

[30]. Yee, E., Lien, F.-S., Keats, A., Hseih, K. J. and D'Amours, R. (2006). *Validation of Bayesian Inference for Emission Source Distribution Using the Joint Urban 2003 and European Tracer Experiments*. Fourth International Symposium on Computational Wind Engineering (CWE2006), Yokohama, Japan, 4 pp.

[31]. Keats, A., Yee, E. and Lien, F.-S. (2007). *Bayesian Inference for Source Determination With Applications to a Complex Urban Environment*. Atmos. Environ., 41, 465–479.

[32]. Keats, A., Yee, E. and Lien, F.-S. (2007b). *Efficiently Characterizing the Origin and Decay Rate of a Non-conservative Scalar using Probability Theory*. Ecological Modeling, 205, 437–452.

[33]. Yee, E. (2008). *Theory for Reconstruction of an Unknown Number of Contaminant Sources using Probabilistic Inference*. Boundary-Layer Meteorol., 127, 359–394.